Effective Date: April 22, 2011
Revision -

GSFC JPSS CMO
07/19/2011
Released

Joint Polar Satellite System (JPSS) Ground Project
Code 474
474-00030

Joint Polar Satellite System (JPSS) VIIRS Active Fires: Fire Mask Algorithm Theoretical Basis Document (ATDB)

For Public Release

The information provided herein does not contain technical data as defined in the International Traffic in Arms Regulations (ITAR) 22 CFC 120.10.
This document has been approved For Public Release.

National Aeronautics and Space Administration

Goddard Space Flight Center
Greenbelt, Maryland

This page intentionally left blank.

Joint Polar Satellite System (JPSS)
VIIRS Active Fires: Fire Mask
Algorithm Theoretical Basis Document (ATDB)

JPSS Electronic Signature Page

Prepared By:

Neal Baker
JPSS Data Products and Algorithms, Senior Engineering Advisor
(Electronic Approvals available online at https://jpssmis.gsfc.nasa.gov/mainmenu_dsp.cfm)

Approved By:

JPSS Ground System

Heather Kilcoyne
JPSS Data Products and Algorithms Manager
(Electronic Approvals available online at https://jpssmis.gsfc.nasa.gov/mainmenu_dsp.cfm)

Goddard Space Flight Center
Greenbelt, Maryland

This page intentionally left blank.

Preface

This document is under JPSS Ground Algorithm configuration control. Once this document is approved, JPSS approved changes are handled in accordance with Class I and Class II change control requirements as described in the JPSS Configuration Management Procedures, and changes to this document shall be made by complete revision.

Any questions should be addressed to:

JPSS Ground Project Configuration Management Office
NASA/GSFC
Code 474
Greenbelt, MD 20771

This page intentionally left blank.

Change History Log

Revision	Effective Date	Description of Changes (Reference the CCR & CCB/ERB Approve Date)
Original	04/22/2011	**474-CCR-11-0045**: This version baselines D43770, VIIRS ACTIVE FIRES: FIRE MASK Algorithm Theoretical Basis Document ATDB (REF P1187-TR-I-001), Rev C dated 09/28/2010 as a JPSS document, version Rev –. This is the version that was approved for NPP launch. Per NPOESS CDFCB - External, Volume V – Metadata, doc number D34862-05, this has been approved for Public Release into CLASS. This CCR was approved by the JPSS Ground Algorithm ERB on April 22, 2011.

This page intentionally left blank.

NATIONAL POLAR-ORBITING OPERATIONAL ENVIRONMENTAL SATELLITE SYSTEM (NPOESS)

VIIRS ACTIVE FIRES: FIRE MASK ALGORITHM THEORETICAL BASIS DOCUMENT ATDB (REF P1187-TR-I-001) (D43770 Rev C)

CDRL No. A032

Northrop Grumman Space & Mission Systems Corporation
One Space Park
Redondo Beach, California 90278

This documentation/technical data was developed pursuant to Contract Number F04701-02-C-0502 with the US Government. The US Government's rights in and to this copyrighted data are as specified in DFAR 252.227-7013, which was made part of the above contract.

This document has been identified per the NPOESS Common Data Format Control Book – External Volume 5 Metadata, D34862-05, Appendix B as a document to be provided to the NOAA Comprehensive Large Array-data Stewardship System (CLASS) via the delivery of NPOESS Document Release Packages to CLASS.

NATIONAL POLAR-ORBITING OPERATIONAL ENVIRONMENTAL SATELLITE SYSTEM (NPOESS)

VIIRS ACTIVE FIRES: FIRE MASK ALGORITHM THEORETICAL BASIS DOCUMENT ATDB (REF P1187-TR-I-001) (D43770 Rev C)

PREPARED BY:
Dr Alain Sei, AM&S FV IP Lead

ELECTRONIC APPROVAL SIGNATURES:

_____

Roy Tsugawa Date
Algorithm & Data Processing IPT Lead &
Algorithm Change Control Board Chairperson

_____

Gerald J. Mulvey Date
Senior Systems Engineer

Revision/Change Record

Document Number D43770

Revision	Document Date	Revision/Change Description	Pages Affected
---	1/26/2007	Initial PCIM Release to bring the document into Matrix Accountability. Reference original document number: Y3252 delivered in 2002 **Obsolete**	All
A	12/18/2007	Release to bring the document into Matrix Accountability. Reference original AER document number: P1187-TR-I-001 delivered in 2003.	All
B	12/1/2008	Modified to accommodate CDA comments. Incorporates ECR A-203. Approved for Public Release per Contracts letter 090618-01.	All
C	9/28/2010	Added comments to respond to document convergence RFA Incorporated ECR-A-334 and removed "OAD" from title pages.	11

Table of Contents

List of Figures

List of Tables

1. Introduction

1.1. Purpose

This document presents the scientific background, algorithm design and algorithm performance of the Fire Mask Algorithm for the National Polar Orbiting Environmental Satellite System (NPOESS). The Fire Mask Algorithm produces a fire/ no fire mask from Visible and Infrared Imaging Radiometer Suite (VIIRS) data. Atmospheric and Environmental Research (AER), Inc. performed this work under contract to the Northrop Grumman Space Technology NPOESS Project.

The VIIRS Fire Mask (VFM) algorithm described here provides one of the three parameters identified in the NPOESS Active Fires EDR specification (40.6.4.1): the latitude and longitude of pixels containing active fires. The algorithm described here produces important additional diagnostic data. The fire mask and associated diagnostic data are both important for subsequent fire processing and have intrinsic value by themselves for many users. For this reason, we treat the VIIRS Fire Mask as an intermediate product (IP).

1.2. Scope

The algorithm and software described here resulted from an accelerated development effort by AER of approximately one month in duration. The goal was to develop and test a VIIRS-compatible Fire Mask based on the latest proven algorithm techniques within a time frame meeting schedule requirements for algorithm migration to the Integrated Data Processing Segment (IDPS) for the NPOESS Preparatory Project (NPP).

We began with the Version 4 MODIS Fire Mask and adapted it to the unique characteristics of the VIIRS sensor. Version 4 is the latest operational version of the MODIS Fire Mask and has benefited from extensive validation and optimization. This approach met the accelerated schedule requirements at low risk and resulted in a high quality, state of the art Fire Mask.

Section 2 of this document presents an overview of the scientific basis of the fire mask algorithm. Section 3 describes the algorithm implementation in detail. Section 7 covers the algorithm testing and provides performance estimates of the product. Section 5 briefly covers some practical aspects of the algorithm implementation. Section 6 contains the references.

1.3. Applicable Documents

Table 1 lists relevant specifications guiding the Fire Mask algorithm development.

Table 1 – Relevant Specifications

Organization	Document	Application
Northrop Grumman Space Technology	National Polar Orbiting Environmental Satellite System (NPOESS) System Specification (1 August 2002), SY15-007	Source of System Requirements
Raytheon Company, Santa Barbara Remote Sensing	Sensor Performance Specification for the Visible/ Infrared Imager Radiometer Suite, 24 January 2002,VIIRS PS15460-101 Revision A	Source of VIIRS Sensor Performance Requirements

The companion document to this scientific algorithm description is:

AER, Inc.: VIIRS Active Fires: Fire Mask – Software Description, 22 August 2003, Version 1.0

which describes the details of the software design and implementation. It also contains user instructions and format descriptions.

1.4. Follow-on Trade Study

This effort will be followed by a trade study evaluating approaches to best meet the System Specification requirement for estimating sub-pixel fire temperature/ area. This trade study will consider:

- Current approaches to deriving active fire temperature and sub-pixel area (i.e., the basic Dozier algorithm using channels at ~11 and 4 μm without any special handling for saturation)
- Sensor and algorithm driven risks, especially saturation and pixel co-registration
- Algorithm changes and low impact sensor changes to mitigate the above risks
- If the risks above cannot be reduced to acceptable levels by the identified trades, alternate products providing similar application utility to end users may be evaluated

The Fire Mask algorithm, software, test data and test infrastructure developed here will be extended and applied to this follow-on task. As part of this initial effort AER has already developed some key components that can be used in the trade study:

- a prototype fire temperature and area algorithm based on Dozier's methods
- tools to evaluate impacts of co-registration, quantization and saturation
- fire simulation tools that generate realistic fires of various types

Included in the trade study will be an examination and comparison of the approach to handling detector saturation outlined in the VIIRS Version 5 ATBD. A key goal of the trade study is to determine if issues and risk with the Version 5 approach (noted in the ATBD and discussed at VIIRS Operational Algorithm Team meetings) can be adequately mitigated.

The results of this trade study will be carefully reviewed with Northrop Grumman, the IPO and other NPOESS stakeholders before a final approach is implemented.

1.5. Relationship to the Sensor Contractor's VIIRS Active Fires Fire Mask

The VIIRS sensor contractor has developed and delivered an Algorithm Theoretical Basis Document and associated science grade code for the Active Fires product. The latest VIIRS contractor algorithm release for fire is at Version 5. A fire mask is one of the included algorithm elements of this software. The Version 5 algorithm is based on the MODIS Version 3 fire mask.

Independent evaluation and testing at Northrop Grumman determined the need to use newer methods developed for MODIS (Giglio, et al, 2003) and represented in the MODIS Version 4 algorithm (these methods were not available until after the VIIRS contractor delivered the VIIRS Version 5 algorithm). This document describes our development of a VIIRS fire mask algorithm based on the MODIS Versions 4.

2. Overview and Background Information

2.1. Objectives of the Fire Mask Algorithm

The purpose of the VIIRS Fire Mask algorithm is to provide an identification of VIIRS pixels with active fires. The primary purpose is to flag pixels containing fire for subsequent processing by the algorithm to derive the pixel's fire temperature and fractional area. Thus, the fire mask is a derived requirement. The minimal objectives are to detect the complete range of fires for which the Active Fire EDR requirement applies (see section 2.3).

In practice, real fires cover a significantly wider range in terms of both temperature and fractional area. Insofar as it will only be after the fact (i.e., after the subsequent fire temperature/ area retrieval) that the fire characteristics will be available to the algorithm, the fire mask testing must consider a wider range of fires.

To accommodate this, the analysis conducted here is over a more comprehensive range of fires. We will report our performance results over several subsets of the fires ranges (given in terms of fractional area and fire temperature). This is important to understand the full range of fires that will eventually be processed by the fire temperature/ area algorithm. It will also be beneficial to other potential users of the fire mask.

2.2. Science Applications

The scientific applications of fire products provide a useful context within which to guide the algorithm development. In addition, these applications were the motivation for inclusion of the Active Fires as a NPOESS requirement.

The scientific rationale presented by Kaufman and Justice (1998) for the MODIS Active Fire Products pertains directly to the NPOESS applications of VIIRS-derived fire products.

Fire is an important terrestrial process with implications to a wide variety of climate, land use management, ecosystem dynamics, atmospheric chemistry, human health and atmospheric particulate research efforts. Fire is an important element in greenhouse gas emissions and the global carbon cycle. Biomass burning affects regional and global distribution of tropospheric ozone. It is also a major source of a wide variety of important trace gases including NO, CO, CO_2, CH_4, N_2O. Aerosols generated by fires have significant importance in many areas including human health, precipitation, and earth radiation budget. The radiation budget effects include direct radiative effects (where heating or cooling is driven by the single scattering albedo of the generated particulates) and indirect effects (e.g. modulation of cloud formation). The effect of fire on the land immediately changes reflectance/ albedo properties with impacts to surface radiation balance. It also affects the water cycle through complex interactions with vegetation canopies and soil. Finally, fire is an important element in the maintenance and evolution terrestrial ecosystems.

The above synopsis indicates that fire is relevant to many NPOESS EDRs not just the Active Fires product. These relevant EDRs include: the earth radiation budget EDRs, albedo, aerosols, clouds, surface type, Normalized Difference Vegetation Index (NDVI) and suspended matter.

The baseline of consistent high quality fire observations made by MODIS will be extended by VIIRS. MODIS currently provides three primary (level 2) fire products:

- Fire detection, locating pixels with likely actively burning fires
- A fire emitted energy product
- A fire burned area product identifying recently burned areas

Of these, only the first is currently a VIIRS requirement. For MODIS production of fire temperature and area estimates remains experimental.

2.3. Derived Fire Mask Requirements

The Active Fire EDR[1] requirements are reproduced from the NPOESS System Specification as given in Table 2 and Table 3. This has been augmented with interpretive comments and discussion of flow-down to the VIIRS Fire Mask derived requirements.

Table 2 – Active Fires Specification Preamble from System Specification 40.6.4.1

Specification Text	Interpretation/ Comments
Active surface fires are natural or anthropogenic fires.	Includes both fires in natural terrain (e.g., forests and grasslands) and man-made fires (e.g. oil well fires and burning man-made structures). However, fire area constraints in the attribute table will eliminate most man-made fires from consideration.
This EDR provides (a) geolocation of the pixels in which active fires are detected, (b) the sub-pixel average temperature of each active fire, and (c) the sub-pixel area of each active fire	Implies a tabular product data format that identifies fires by pixel geolocation (latitude/ longitude) and sub-pixel fire's temperature and area.
A global, binary "fire/no fire" map is neither required nor desired.	We interpret this to simply mean that a binary map-type product format is not desired (where every pixel in a scene is tagged as fire or no-fire. A fire mask is implied by the above paragraph which also states the preferred data structure for delivery.
The products for this application are desired during both day and night time …	Required on all platforms at all times.
… for clear-sky conditions and within clear areas under conditions of broken clouds.	We interpret clear sky and broken clouds to refer to the cloudiness characteristics of the area surrounding a given pixel. The actual retrievals will be performed only for clear pixels as identified by the VIIRS Cloud Mask (VCM).
Units: Degrees latitude and longitude for geolocation, K for sub-pixel average temperature, m^2 for active fire area.	States required units

Table 3 -- Active Fires Specification Attribute Table from System Specification 40.6.4.1

Paragraph	***Subject***	***Specified Value***	***Interpretation/ Flow-down***
	a. Horizontal Cell Size		
40.6.4.1-1	*1. At Nadir [VIIRS Guarantee]*	*0.75 km*	*Direct flow-down to VFM*
40.6.4.1-2	*2. Worst Case [VIIRS Guarantee]*	*1.6 km*	*Direct flow-down to VFM*
40.6.4.1-3	*b. Horizontal Reporting Interval [VIIRS Guarantee]*	*HCS*	*Direct flow-down to VFM*

[1] Active Fire is referred to as an Environmental Data Requirement (EDR) in the NPOESS System Specification. The Raytheon VIIRS System Specification and the IPO's NPOESS Technical Requirements Document both refer to fire as an Application Related Requirement (ARR). From a requirements perspective this difference in terminology is not significant: it is a contractually-required data product.

Paragraph	***Subject***	***Specified Value***	***Interpretation/ Flow-down***
40.6.4.1-4	*c. Horizontal Coverage [VIIRS Guarantee]*	*Land*	*Direct flow-down to VFM*
	d. Measurement Range		
40.6.4.1-5	*1. Sub-pixel Average Temperature of Active Fire [VIIRS Guarantee]*	*800 K – 1200 K*	*Direct flow-down to VFM* *Note: Effective fire temperatures considering both flaming and smoldering components will often be less than this*
40.6.4.1-6	*2. Sub-pixel Area of Active Fire [VIIRS Guarantee]*	*From 1000 m^2 to 50 m Times Ground Sample Distance in Scan Direction*	*Direct flow-down to VFM* *(See Note A)*
	e. Measurement Uncertainty		
40.6.4.1-7	*1. Sub-pixel Average Temperature of Active Fire [VIIRS Guarantee]*	*50 K*	*Not flown-down to VFM*
40.6.4.1-8	*2. Sub-pixel Area of Active Fire [VIIRS Guarantee]*	*30%*	*Not flown-down to VFM*
40.6.4.1-9	*f. Mapping Uncertainty, 3 Sigma [VIIRS Guarantee]*	*1.5 km*	*VFM will use geolocation provide by SDR algorithm*
40.6.4.1-11	*g. Maximum Local Average Revisit Time*	*3.9 hrs*	*Implies VFM is required on 3-satellites for full VIIRS swath (~ 3,000 km)*
40.6.4.1-13	*h. Latency*	*See Appendix E*	*System and IDPS requirement – not flown down to VFM*
40.6.4.1-14	*i. Excluded Measurement Condition: Aerosol Optical Thickness > 1.0 [VIIRS Exclusion]*		*Direct flow-down to VFM*
Note A – There is an ambiguity in this specification as to whether the maximum size (50 m times the ground sample distance in the scan direction) specifies not just the area but also the orientation of the fire. This is significant with regard to the saturation characteristics of the VIIRS sensor because of its sub-pixel aggregation. A fire that lies across multiple sub-pixels will be less prone to saturate as it spans multiple sub-pixels. A fire entirely within a sub-pixel will be more prone to saturate (i.e. will saturate at lower fire temperature and/ or areas). The current assumption is that this specification implies a specification for the fire area and does not imply a particular orientation. These assumptions have little impact on fire detection but will affect the fire temperature and area quantification.			

It should be noted that the fire algorithms under consideration essentially detect thermal anomalies. Volcanoes/ lava flows will also be flagged as fires. We will treat such anomalies as fires providing they meet the temperature/ area specifications above.

2.4. Physics of the Problem

Active fires cause thermal anomalies (excess thermal radiation over the background) in pixels containing high temperatures resulting from actively flaming and/or smoldering sub-pixel areas. The

extent of the anomaly varies with wavelength depends on both the sub-pixel fire area and effective temperature.

The non-linear properties of the Planck function result is a much higher sensitivity of the observed radiance to sub-pixel fires at wavelengths in the mid-wave infrared (near 3.7-4 μm) than in the long-wave infrared (near 10-12 μm). This is illustrated in Figure 1 which shows the observed brightness temperatures at 4 μm (corresponding to VIIRS M13) and 10.6 μm (corresponding to M15) at three different fractional areas (f = 0.01,, 0.5, 0.1) versus fire temperature. The brightness temperature of the non-fire background is 190 K in all cases. The upper three lines with the greatest sensitivity to fire are for the M13 bands, while the lower three are for M15. Note that a smaller fire at M13 (f= 0.01) has nearly the same sensitivity as a large fire at M15 (f=0.1). The brightness temperatures differ significantly from the background at M13 for warmer fires. This is the preferred signature for fire detection.

For lower temperature fires (< 600K), especially if small (f ≤ 0.01), the difference from the background may not be significant enough to detect from the background clutter. In this case a different signature is exploited: the brightness temperature difference between 4 and 11 μm. This is shown in Figure 2. Even for smaller cooler fires, brightness temperature differences can be > 10 K.

A number of confounding signatures exist from other phenomena that can be confused with fires: clouds particularly in the daytime (delta T signature), sun glint, very warm natural surfaces (asphalt, hot sand). The strategy for fire detection can now be seen: use absolute tests for fire detection for warmer larger fires. For cooler, smaller fires screen out potentially confounding conditions (e.g., sun glint) and employ a contextual search to estimate the natural local variability (without fire) of the two signatures. Flag pixels as fire that are sufficiently above this natural variability.

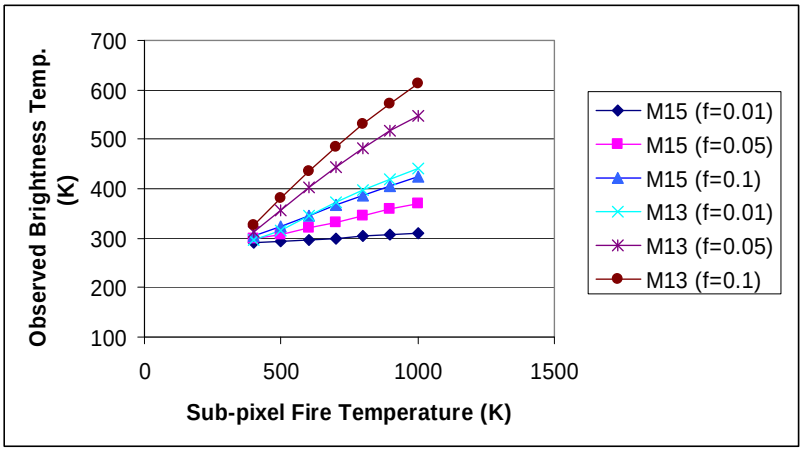

Figure 1 – Sensitivity of 10.6 μm (M15) and 4 μm (M13) to fire temperature and size

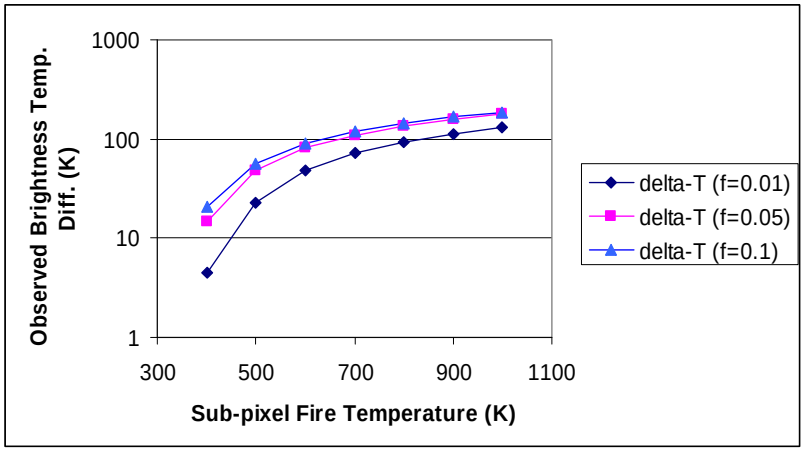

Figure 2 – Sensitivity of M13-M15 brightness temperature difference to fire temperature and size

2.5. Instrument Characteristics

The VIIRS instrument characteristics are described in detail elsewhere (see Section 2.2 of the Raytheon Active Fires ATBD) and are not repeated here.

Table 4 compares the MODIS and VIIRS sensor characteristics relevant to fires.

Table 4 – Comparison of MODIS and VIIRS Instrument Characteristics Relevant to Fire

Property	MODIS (Terra)	VIIRS	Comments
Number of pixels/swath (scene samples)	10 X 1354	16 X ~3162	Slightly larger swaths for VIIRS, not significant to algorithm
Number of swaths/granule	203	May not employ a granule processing paradigm (NPOESS's variable and short contact periods will affect this)	Geometric contextual search approaches will need at least two swaths in memory at any time to produce fire mask
Resolution	NAD: 1 X 1 km EOS: 2 x 6 km (approx.)	NAD: 0.75 x 0.75 km EOS 1.6 x 1.6 km	Improved resolution of VIIRS will improve fire detection capability, especially near edge of scan
Aggregation	None	Aggregation of sub-pixels varies across scan (to minimize geometric distortion of final output pixels) Some channels are aggregated on-board (single gain and Day Night Band)	Very small sub-pixels near nadir will increase frequency of saturation – saturation is much less significant for the fire mask as compared to the fire temperature/ area product

		and some on the ground (dual gain) Aggregation varies from 3 along-scan sub-pixels near nadir, to 2 sub-pixels in intermediate portion of scan to 1 (i.e., no aggregation near edge of scan)	
Bowtie overlap image artifact	No masking applied	Modified bow-tie deletion: Some (but not all) overlapping pixels deleted from downlinked data stream – assumed replaced with fill values in SDR processing	Contextual search algorithm must be account for geometric overlap (already part of MODIS V4 algorithm) VIIRS adaption needs to consider both the geometric overlap and the bow tie deletion
Bands and dynamic range	Thermal bands: M21 3.96μm 1 km 331 K M22 3.96μm 1 km 500 K M31 11.03μm 1 km 340/400 K M32 12.05μm 1 km 400 K Reflectance bands (averaged to 1 km): M01 0.64μm 250m M02 0.86μm 250m M07 2.13μm 500m	Thermal bands: M13 4.05μm 742m 634 K M15 10.76μm 742m 343 K M16 12.01μm 742m 340K Reflectance bands: M05 0.67μm 742m M07 0.86μm 742m M11 2.13μm 742m	VIIRS has adequate bands Excellent dynamic range for 4 μm band. Much reduced VIIRS dynamic range of 10.76 μm band (compared to MODIS) has limited impact on fire detection

The saturation and sub-pixel aggregation interact in subtle ways that effect fire processing.

The M15 (the 10.76 μm band) is a single gain band and is aggregated on-board. Inquiries to Raytheon SBRS indicate that the expected processing method will pin the value at the maximum counts for the sub-pixel readout. This pixel is then averaged with the counts from the neighboring pixels (used to form the down-linked pixel). Should these neighboring pixels not be saturated, then the resulting down-linked counts would be lower (and perhaps significantly lower than the maximum (2^{12} –1). An entirely plausible situation would be that near nadir one pixel is saturated (small hot fire) and the neighboring sub-pixels are near the background temperature. In such a case, it would be entirely plausible for the resulting pixel to output a value as low as 300K brightness temperature. It is important to note that the radiometric output in this case is no longer valid (i.e., it does not represent the average radiance over the pixel). The low value of the M15 saturation means that this will be a frequent occurrence when fires are present.

Since the M13 (4 μm channel) is aggregated on-board the actual aggregation is part of the RDR-to SDR processing (referred to as the SDR processing) and is being implemented by the IDPS Team. We note that overall utility of the data relative to saturation would be improved by very simple changes to the ground and on-board processing. Basically, in the case that any sub-pixel is saturated, the output would be replaced by the saturated counts (and not the average of all sub-pixels). This change would be very easy to implement in the ground processing for channel M13. As it would

require changes to the VIIRS on-board signal processing hardware and/ or firmware this would be more involved and likely not feasible for the NPP flight model.

As will be shown in section 3.4, the net effect of saturation is very small on the fire detection algorithm. This is not the case, however, for the fire temperature/ area product (to be evaluated in more detail in the follow-on trade study).

3. Algorithm Description

3.1. Algorithm Overview

Our delivered algorithm is based on the MODIS Version 4 Fire Mask. This algorithm and including the changes since MODIS Fire Mask Version 3 is described in detail in Giglio, et al (2003).

Justice (2002) summarizes the impacts of the Version 4 changes on the MODIS products. Most significantly, there was a much-reduced occurrence of false alarms.

Appendix A compares the VIIRS Version 5 fire mask algorithm (based on the MODIS Version 2/3 fire mask), the MODIS Version 4 fire mask and the changes implemented to our delivered fire mask.

The following are the major changes implemented to adapt the MODIS Version 4 fire mask to VIIRS:

- Adapt contextual search to work with VIIRS-unique features (see below)
- Modify algorithm to work with a single 4 μm band as compared to the two bands for MODIS
- Place all algorithm parameters in a configuration file
- Add options to use internal cloud mask (as per MODIS Version 4 FM) or external mask (the external mask uses the reformatted MODIS cloud mask)

The purpose of the contextual search step of the algorithm is to gather local clutter statistics for the contextual threshold tests. Earlier versions of MODIS and VIIRS Version 5 simply employed a 2-dimenstional search in the along- and cross-track direction in the internally stored array. This results in an irregular sampling including sampling of non-adjacent pixels, multiple sampling of pixels, etc. MODIS Version 4 includes a "bow-tie" aware search algorithm that correctly searches for pixels that are geometrically adjacent.

3.2. Algorithm Description

The functional flow of the VIIRS fire detection algorithm is illustrated in Figure 3. The input parameters are described in Table 5 which covers the semantic content of the inputs. See the software documentation for a description of the exact formats. Table 6 summarizes the output data (see software documentation for detailed list of data and bit mappings).

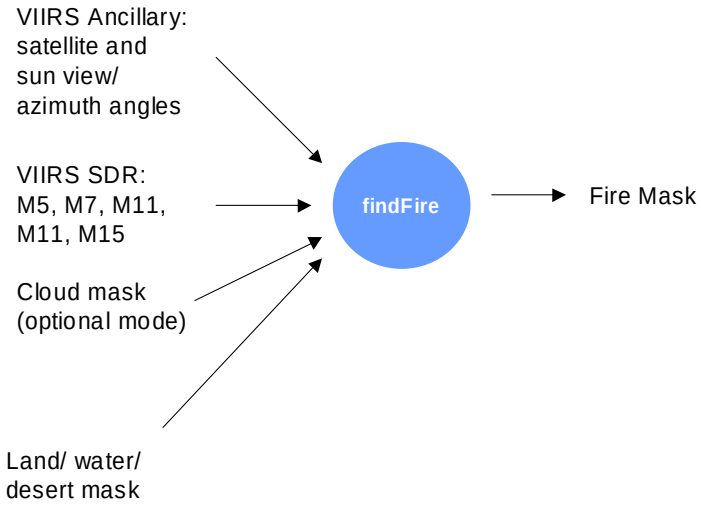

Figure 3 - Fire Mask Algorithm Functional Flow

Table 5 – Fire Detection Inputs

Type	Description	Units	Source	Comments
SDR	Reflectances: M5, M7, M11	Unitless	VIIRS SDR algorithm (radiometric calibration)	See text below table 7 for comments on SDR interface
	Brightness temperatures: M13, M15, M16	Degrees K	VIIRS SDR algorithm (radiometric calibration)	See text for comments on SDR interface
Auxiliary	Pixel latitude, longitude	Degrees	VIIRS SDR algorithm (geolocation)	
	Scan zenith angle and azimuth (local at pixel on ground)	Degrees	VIIRS SDR algorithm (geolocation)	Azimuth relative to true north
	Solar zenith and azimuth	Degrees	VIIRS SDR algorithm (geolocation)	Azimuth relative to true north
Ancillary	Land/ water mask	Unitless	Static database, with characteristics & quality similar to GeoTopo 30	Only subset of parameters used: land, water and ephemeral water flags

Table 6 – Fire Detection Outputs

Name	Type	Description
Fire_Mask	Byte (8-bit) mask for every pixel in a swath	8-bit mask classifies pixels as not processed, cloudy, water, unknown, low confidence fire, normal confidence fire, high confidence fire
Fire_QC	32-bit word bit mask	Bits designate the state of all key algorithm tests used in classifying the pixel.
Fire_Diagnostics	Total of 23 words (either 32 bit integers or floats)	Additional diagnostic data for all pixels classified as fire including relevant radiances/ reflectances, information on surface characteristics, contextual window size, cloud information, contextual background statistics

The software implementation of the algorithm described here (see the software documentation) has the following features:

- Data are input as scaled integers linear in radiance and un-normalized reflectance. The input data file also includes the coefficients to transform the scaled integers to radiance and un-normalized reflectance. This is similar to the strategy adopted for MODIS.
- Un-normalized reflectance is defined as $\rho'_\iota = \pi L_i / F_0$, where L_i is the measured radiance and F_0 is the top of atmosphere solar irradiance integrated over the sensor spectral bandpass.
- Reflectance (or normalized reflectance) used in the algorithm is computed from the above values. It is defined as = 0 for SZA ≥ 85 degrees (to avoid the singularity at SZA = 90 degrees) and as $\rho_\iota = \rho'_\iota / \cos(\mathrm{SZA})$ for SZA ≤ 85. The reflectance are available directly from the VIIRS SDR so no normalization is needed in the fire code.
- Thermal bands (M13, M15, and M16 for this algorithm) input the data as radiances from the SDR file. They are converted to brightness temperatures in the program. The wide dynamic range and finite band passes mean that a simple inverse Planck function is not sufficiently accurate to convert radiances to brightness temperatures. The brightness temperature routine included with the delivered algorithm code accounts for the finite bandpass. In general, the parameters controlling the brightness temperature calculation will vary from sensor to sensor.

See the software documentation for additional details on the SDR interface and considerations for migration to operational code. Note also that the output of the operational VIIRS active fire code is the list of latitude and longitude of fire pixels.

The operations leading to the fire detection mask are presented in Table 7. The algorithm processes each scan (i.e., 16 pixels wide for VIIRS) in turn but uses information from the adjacent scans (the preceding and subsequent scans) for the purpose of computing background statistics. Within each scan all valid pixels (i.e., those not subject to bow-tie deletion) are processed.

Table 7 – Algorithm description

The following definitions apply to the algorithm description:

T_i is the brightness temperature for channel i

ΔT is $T_{13} - T_{15}$

ρ_i is the reflectance (including normalization by solar zenith angle)

& is logical 'AND'; | is logical 'OR', ~ is logical not

DAY is defined as solar zenith reference angle (SZA) at reference pixel > 85 degrees, NIGHT = ~ DAY

The glint angle is the cone angle between the solar specular reflectance vector and the satellite view vector to pixel

1. Identify potential fire pixels

a. Pre-screen pixels, select pixels satisfying all of the below
   i. Pixel has a valid SDR and is not a fill value (=NOT_FILL) E.g. as arises when a pixel deleted on-board as part of bow tie deletion is replaced with a fill value on the ground as part of RDR-to-SDR processing.
   ii. Pixel is land or ephemeral (intermittent) land (= LAND)
   iii. Pixel is classified as clear cloud mask (=CLEAR) (internal mask is default, see Section 3.2.1)

b. Select potential pixels
   i. Daytime: Identify pixels with $T_{13} > 310$, $\Delta T > 10$, and $\rho_7 < 0.30$
   ii. Nighttime: Identify pixels with $T_{13} > 305$ and $\Delta T > 10$

2. Generate contextual statistics

a. Conduct search in geometric neighborhood of potential fire pixel, ranging from 3x3 pixel box (centered at the potential fire pixel) to 21x21 pixels. The search needs to consider geometrically adjacent pixels and the inclusion of fill values replacing pixels deleted on-board as part of bow-tie deletion. The search considers all pixels in the neighborhood except the pixels on the same scan line and adjacent (left and right) to the potential fire pixel. Set VALID_SEARCH = FALSE. For each neighborhood size from 3x3 to 21x21, do the following.

i. For each pixel in the geometric neighborhood

1. Determine if valid background pixel as VALID_BKGND = (DAY & T_{13}> 325 & ΔT > 20) | (NIGHT & T_{13}> 310 & ΔT > 10) & CLEAR & NOT_FILL & LAND. Otherwise flag pixel as a background fire.
2. Accumulate data for statistics on T_{13}, T_{15} and ΔT

ii. Compute:

1. N_t = number of non-fill pixels in neighborhood search
2. N_b = number of valid background pixels in neighborhood search
3. fraction valid background pixels: $F_b = N_b / N_t$

iii. If ($F_b \geq 25\%$ and $N_b \geq 8$) then set VALID_SEARCH = TRUE and exit neighborhood search loop; else search over next larger region

b. Test VALID_SEARCH flag: If FALSE, then flag pixel as unknown and continue with next pixel for fire test; else proceed to next step

c. Compute aggregate statistics over selected search region:

i. Compute mean of valid background pixels (T_{13B} ,T_{15B} ,ΔT_B)

ii. Compute mean absolute deviation of valid background pixels (δT_{13B} , δT_{15B} , $\delta \Delta T_B$)

iii. Compute mean absolute deviation of background fires (T'_{13B}, $\delta T'_{13B}$)

3. Compute absolute fire test

a. TEST_1 = (DAY & $T_{13} > 360$) | (NIGHT & $T_{13} > 320$)

4. Compute contextual fire tests

a. TEST_2 = $\Delta T_B + 3.5\ \delta \Delta T_B$

b. TEST_3 = $\Delta T > \Delta T_B + 6$

c. TEST_4 = $T_{13} > T_{13B} + 3\ \delta T_{13B}$

d. TEST_5 = $T_{15} > T_{15B} + \delta T_{15} - 4$

e. TEST_6 = $\delta' T_{13B} > 5$

5. Compute fire mask

i. DAY_FIRE = DAY & (TEST_1 | (TEST_2 & TEST_3 & TEST_4 & (TEST_5 | TEST_6)))

ii. NIGHT_FIRE = NIGHT & (TEST_1 | (TEST_2 & TEST_3 & TEST_4))

iii. IS_FIRE = DAY_FIRE & NIGHT_FIRE

6. Reject detected fires if any of the following is satisfied.

a. Glint rejection: Reject fires based on any one glint angle Θ_g criteria

i. $\Theta_g < 2$

ii. $\Theta_g < 8$ & $\rho_5 > 0.1$ & $\rho_7 > 0.2$ & $\rho_{11} > 0.12$

iii. $\Theta_g < 12$ & $(N_{aw} + N_w) > 0$, where N_w is the number of water pixels in search box and N_{aw} is the number of water pixels within 8 pixels of candidate fire pixel

b. Coastal rejection: Identify unmasked water pixels in search box where $\rho_{11} < 0.05$ & $\rho_7 < 0.15$ & NDVI < 0. Reject fires if the number of unmasked water pixels $N_{uw} > 0$ and absolute fire test is false. (NDVI is calculated internally to the algorithm as $(\rho_7 - \rho_5)/ (\rho_7 + \rho_5)$

c. Override detection if it is likely that this is a false alarm caused by excessive rejection of legitimate background pixels based on the following criteria.: $F_b > 0.9$ & $N_b > 3$ & $T'_{13B} < 345$ & $\delta T'_{13B} < 3$ & $\rho_7 > 0.15$ & $T_{13} < (T'_{13B} + 6\delta T'_{13B})$

7. Write out mask and diagnostic (QC) fields

3.2.1. Internal Cloud Mask

Three tests are used internally in the fire detection algorithm to identify clouds.

Cloud Test 1: $(\rho_5 + \rho_7) > 0.9$ (bright surface)

Cloud Test 2: $T_{16} < 265$ K (cold surface)

Cloud Test 3: $(\rho_5 + \rho_7) > 0.7$ AND $T_{16} < 285$ K (bright/cold surface)

If any one of these tests is satisfied, then the pixel is flagged as cloudy. Note that it is not necessary to produce a mask that gives a complete representation of the cloud. Rather it is sufficient for these tests to discriminate between clouds and potential fires so as to not prevent the detection of fires. Our tests as well as those of the MODIS Fire Mask Team indicate that this subset of cloud tests adequately meets these criteria. Moreover, the fire mask generated based on independent cloud criteria could be included as an input to the VIIRS cloud mask algorithm.

3.3. Algorithm Processing Flow

The algorithm processing flow in the test environment is shown in the Figure 4.

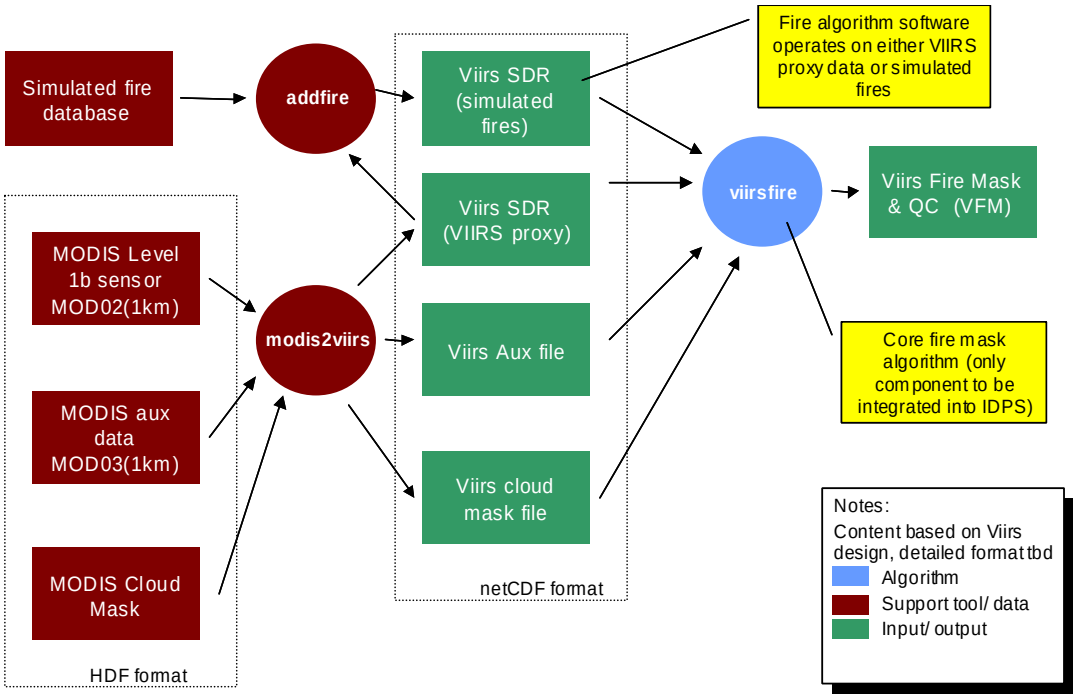

Figure 4 – Algorithm Interfaces.

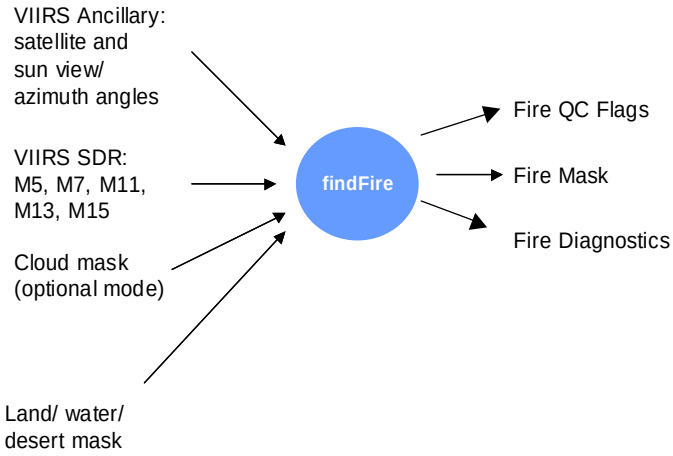

Figure 5 – Algorithm Context Diagram.

An algorithm context diagram is shown in Figure 5; see the software documentation for a detailed pseudo-code description of the algorithm flow.

3.4. Algorithm Sensitivity Studies

3.4.1. Saturation Analysis – Part 1: Dependence on Fire Orientation, Size and Temperature

It is important to consider the effect of the sub-pixel aggregation on saturation of the infrared bands used for fire processing: M13 (4 μm) and M15 (10.6 μm). Saturation will be of greatest concern near nadir where the pixel and sub-pixel sizes are smallest. This is considered below.

Table 8 and Table 9 show the saturation characteristics for VIIRS channels M13 and M15. The references to thresholds and objectives are from the NPOESS TRD. The third and fourth columns correspond to the maximum fire size in the current specification for two orientations (across the scan and perpendicular to the scan).

Table 8 shows that channel M13 does not saturate for any of the range of fire temperatures when the fire is oriented across to the scan, but it does for fires with temperature greater than 636 K when oriented perpendicular to the scan. Since actual fires will fall between these two extremes, the conclusion is that some fires meeting the maximum fire size will saturate M13 for temperatures greater than 900 K.

Table 9 shows that Channel M15 saturates for all fires of the maximum size regardless of orientation and temperature. The impact of this on fire detection is detailed in the follow trade study, see Kennelly, Hogan, Zaccheo, 2004.

Table 8– Saturation Analysis for M13 (shaded indicates not saturated, no shading indicates saturated)

M13 Dual 4.050 μm		OBJECTIVE FIRE SIZE →				
		← THRESHOLD FIRE SIZE →				
T_{sat}= 634 K T_{min}= 268 K		100 m² / 262*742 m² 0.000514	50*50 m² / 262*742 m² 0.012860	50*262 m² / 262*742 m² 0.067390	50*742 m² / 262*742 m² 0.190800	100*742 m² / 262*742 m² 0.381700
FIRE TEMPERATURE (K)	800.	316.	407.	499.	584.	658.
	850.	320.	419.	518.	610.	692.
	900.	324.	430.	537.	636.	725.
	950.	328.	441.	554.	661.	758.
	1000.	332.	452.	571.	685.	790.
	1050.	336.	462.	588.	709.	821.
	1100.	339.	472.	603.	732.	852.
	1150.	343.	481.	619.	755.	883.
	1200.	347.	490.	634.	777.	913.
Illustrations		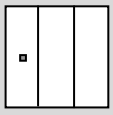	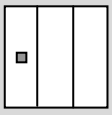	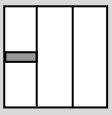	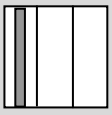	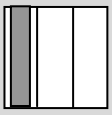

Table 9 – Saturation Analysis for M15

M15 Single 10.763 μm T_{sat}= 343 K T_{min}= 116 K		OBJECTIVE FIRE SIZE				
		THRESHOLD FIRE SIZE				
		$\frac{100\ m^2}{262*742\ m^2}$	$\frac{50*50\ m^2}{262*742\ m^2}$	$\frac{50*262\ m^2}{262*742\ m^2}$	$\frac{50*742\ m^2}{262*742\ m^2}$	$\frac{100*742\ m^2}{262*742\ m^2}$
		0.000514	0.012860	0.067390	0.190800	0.381700
FIRE TEMPERATURE (K)	800.	301.	316.	369.	455.	558.
	850.	301.	318.	376.	470.	582.
	900.	301.	320.	383.	484.	605.
	950.	301.	322.	390.	499.	629.
	1000.	301.	324.	397.	513.	652.
	1050.	301.	326.	404.	527.	675.
	1100.	301.	328.	411.	541.	698.
	1150.	301.	329.	418.	554.	721.
	1200.	301.	331.	424.	568.	743.

M15 does not saturate for fires of the minimum size of the specification (1000 m2). However, it will saturate for fires approximate 3x the minimum fire size at nadir. This effect is much less at the end of scan.

Next to be considered is the ability to detect saturation when it occurs. Figure 6 shows the observed brightness temperature when only one of the aggregated sub-pixels saturates for band M15. The x-axis is the average brightness of the non-saturating sub-pixels. The case of 1-pixel aggregation is the degenerate case where the observed brightness temperature equals that of saturation. For the other two cases, it depends on the brightness temperature of the non-saturating sub-pixels. As can be seen from the figure, for a plausible range of non-saturating sub-pixel brightness temperatures, the observed brightness temperature can be as low as 305K when one sub-pixel saturates. This indicates that it will not be possible with any certainty to know when any one of the sub-pixels saturates by merely looking at the radiance of the aggregated pixel. The on-board processing for VIIRS (which aggregates band M15) does not currently flag saturation in the downlink stream and so the aggregated radiance is the only information available in the current design. This is not expected to have any significant impact on fire detection. Our fire simulations included this effect as part of the simulation and it was shown to be negligible (see section 3.4.2). It may be more serious for the fire temperature area product. This will be considered in the planned trade study Kennelly, Hogan and Zaccheo, 2004.

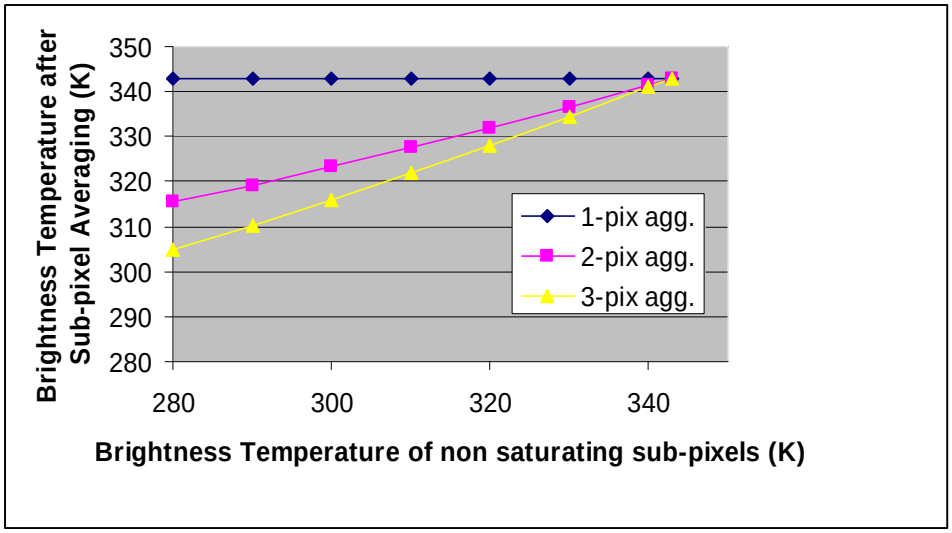

Figure 6 – Observed Brightness Temperature when one of the Band M15 sub-pixels saturates

The high saturation temperature of band M13 and the fact that aggregation is performed on the ground for this band reduces the seriousness of this effect for M13. It is recommended that the ground SDR processing for band M13 (and probably the other dual gain bands as well) separately flag cases where any one sub-pixel saturates.

Recognizing that saturation of M15 will be frequent and M13 much less so, we make the following observations:

1. The impact of saturation on fire detection (the subject of this report) is expected to be small
2. The impact of saturation on determination of sub-pixel fire temperature and area is expected to be large

Item (1) is addressed in more detail as part of algorithm testing (Section 4), but the essential factors are:

- Any fire where M15 saturates will be in a mode where only M13 is used for the detection.
- Even when M13 saturates it will correctly flag a pixel as fire (the only potential confounding natural signature are from volcanoes)

Item (2) is not covered in report, but is addressed in the follow-on trade study Kennelly, Hogan and Zaccheo, 2004 (See Section 1.4). This algorithm requires two appropriately placed bands that both provide high quality radiometry of a pixel. It will not work if either of the two bands is saturated. The only established techniques require bands near 11 and 4 μm. Other proposed methods using different bands have unresolved risks (see VIIRS Version 5 ATBD).

3.4.2. Saturation Analysis – Part 2: Parametric Analysis

A more detailed parametric analysis of detector saturation is shown in Figure 7. This figure shows contours of constant fire fraction (blue lines) and temperature (black lines) on a plot of M13 brightness temperature versus M13-M15 brightness temperature difference. Also shown are the saturation levels for the two channels (red lines) and the thresholds for band M13 for possible fire (green) and absolute fire (dashed green). The portion of the measurement range given in the

NPOESS Specification is shaded in purple. For the region above the upper dashed green line, the absolute fire test is employed and band M15 is not used in the fire algorithm.

Several conclusions can be drawn from the figure:

- For the required measurement range (shaded purple), all portions where band M15 saturates employ the absolute fire test and thus this band is not used in the detection algorithm. Thus, detection of fires within this range is not affected by band M15 saturation.
- The conditions where a fire exists and band M15 is used (i.e., in the contextual and difference tests) are shown to the left of the red M15 saturation line and below the green dashed line. These correspond to large cool fires (temperature <400K). Such regions are more typically characterized as smoldering and they constitute a continuum ranging down to ambient temperature.
- The saturation may affect the statistics generated by the contextual search algorithm. This effect is expected to be small. We have performed tests to evaluate this effect which are discussed in Section 4.6

3.4.3. Quantization

We evaluated the magnitude of quantization for the two key bands: M13 and M15. These bands are down-linked at 12 bit quantization (as are all VIIRS bands except the DNB).

This is shown in Figure 8 for the 4 μm band (MODIS is shown for comparison). M13 is a dual gain band with two separate ranges designated as M13a and M13b. MODIS Terra parameters are used. MODIS uses two separate bands instead of dual gain approach. As can be seen, the lower dynamic range bands for MODIS and VIIRS have very similar quantization. For the upper dynamic range, the VIIRS band has a larger quantization level (almost 1 K at the low end). This level was introduced in all simulations and testing described in section 4. Because of the nature of fire detection algorithm, this larger quantization is not expected to have a significant effect. This was confirmed in the testing described in section 4.

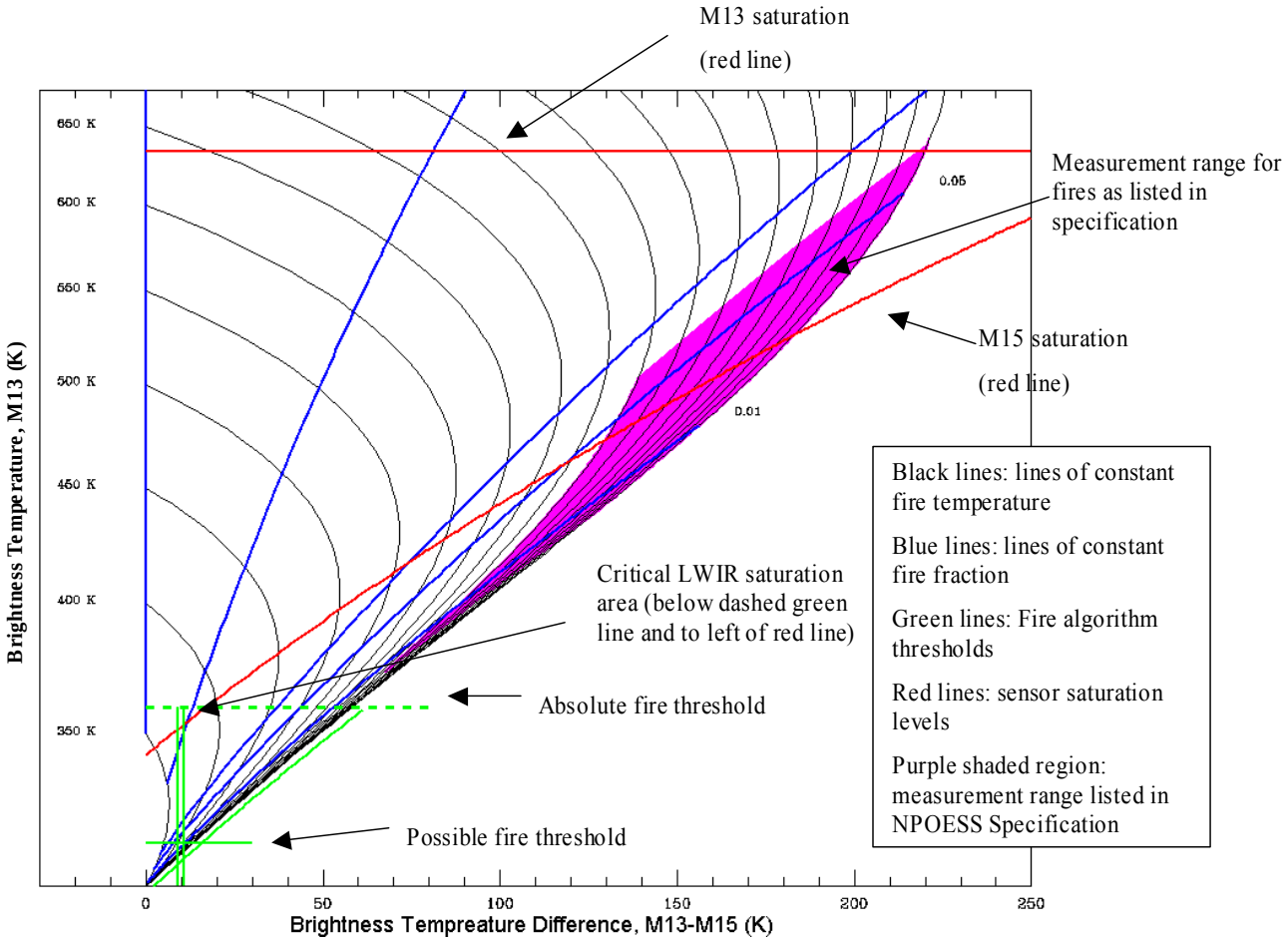
M13 saturation
(red line)
Measurement range for fires as listed in specification
M15 saturation
(red line)
Black lines: lines of constant fire temperature
Blue lines: lines of constant fire fraction
Green lines: Fire algorithm thresholds
Red lines: sensor saturation levels
Purple shaded region: measurement range listed in NPOESS Specification
Critical LWIR saturation area (below dashed green line and to left of red line)
Absolute fire threshold
Possible fire threshold
0.05
0.01
650 K
600 K
550 K
500 K
450 K
400 K
350 K
0
50
100
150
200
250
Brightness Temperature, M13 (K)
Brightness Tempreature Difference, M13-M15 (K)

Figure 7 – Nomogram showing contours of constant fire fraction (blue lines) and temperature

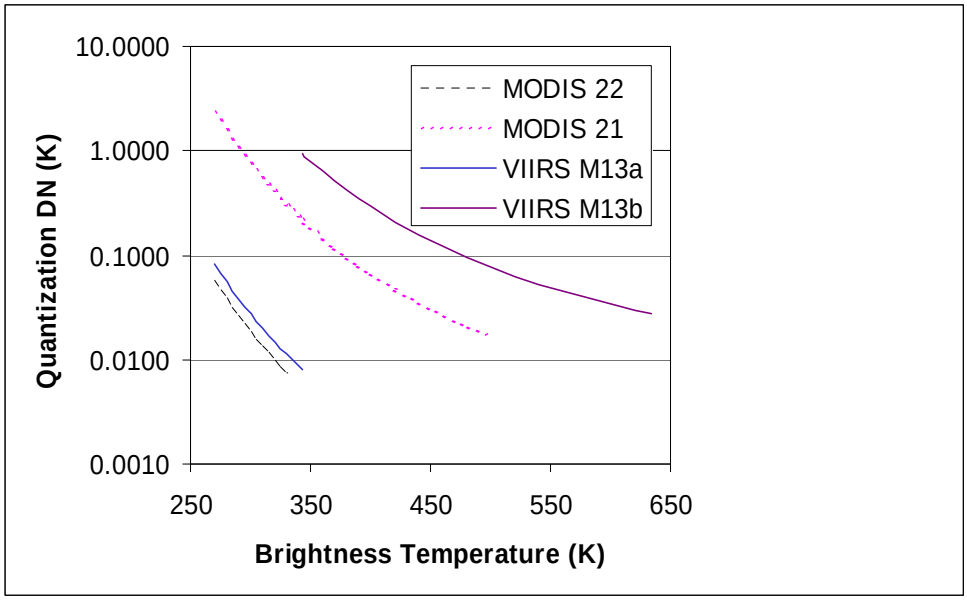

(black lines)

Figure 9 shows the quantization for VIIRS and MODIS for the long-wave infrared band used for fire for each sensor. VIIRS has significantly smaller quantization than MODIS Terra as a consequence of its dynamic range. This will lead to improved characteristics of products such as sea surface temperature which are sensitive to the quantization level.

Figure 8 – Quantization levels for 4 μm MODIS and VIIRS bands (M15a and b are the low and high dynamic range bands respectively

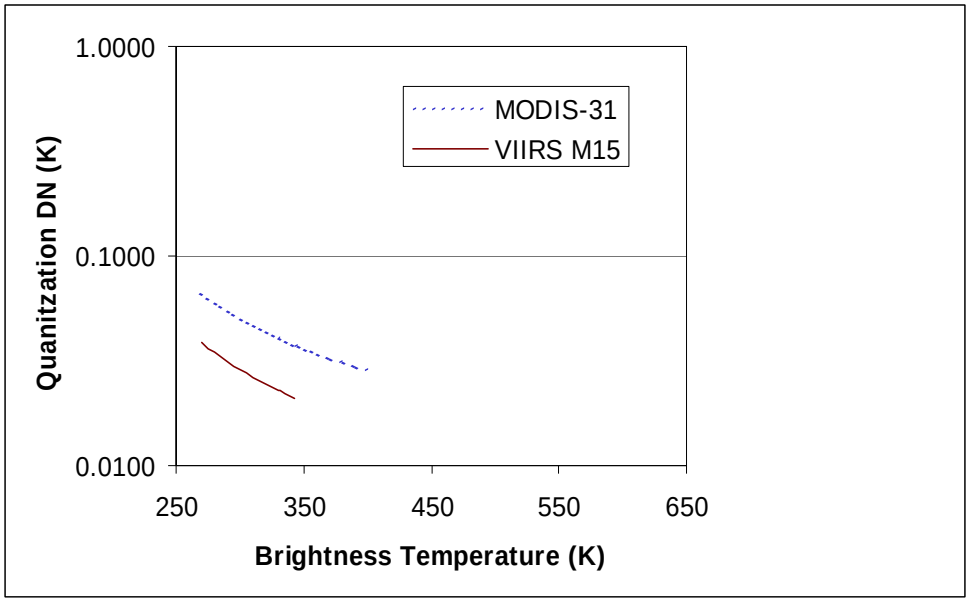

Figure 9 – Quantization levels for 15 μm MODIS and VIIRS bands

4. Algorithm Performance

4.1. Algorithm Test Approach

Testing with real fires was based on scenes obtained from MODIS. All data is processed through the MODIS2VIIRS conversion toolkit to generate SDR and auxiliary data in a common netCDF format that has been adopted for the project.

The delivered algorithm is configured to support the test methods of Table 10. The testing described in this document uses the first 3 scenarios. Northrop Grumman is planning additional testing using their modeling and simulation system to address the last test scenario.

The Real MODIS test mode permits direct comparison to MODIS code and published MODIS products and verification of proper algorithm implementation. The Real VIIRS Proxy mode adapts the data to include critical sensor effects in the context of real background and fires. This permits rapid wide scale testing. The bow tie effect and deletion are appropriate for the 10-lines per scan of MODIS. The simulated VIIRS proxy, permits us to further control the actual fire characteristics using a tool developed AER to simulate the growth and properties of fires. This mode is ideal for trade and sensitivity studies. The use of real MODIS data for the background (non-fire), ensures realistic spatial variability and structure is used. Northrop Grumman is planning additional testing using complete bottoms up simulation (scenario 4). A fifth test method is comparison to ground truth. We envision this will be an important part of the NPP Cal/Val program. Such testing is currently being performed for the MODIS fire mask. When these data are publicly released, it would be beneficial to test this version of the VIIRS algorithm against selected subsets of the validated ground truth data prior to the NPP Cal/ Val.

No single test mode is adequate to fully validate and understand algorithm performance. The use of the multiple test modes adds to the confidence of the algorithm performance estimates.

Table 10 – Test Scenarios Supported by Delivered Algorithm

Item #	Test Data Type	Lines per Scan	Bowtie Deletion	MWIR bands	Description	Purpose
1	Real MODIS	10	No	2 bands	Retains all MODIS data characteristics, reformatting only	Verify proper algorithm implementation and reference for other tests
2	Real VIIRS Proxy	10	Yes	Dual gain	Modify MODIS data to include saturation of band M15, quantization of band M13 and "modified bow tie deletion"	Real data adjusted to closely approximate VIIRS sensor characteristics relevant to fire detection
3	Simulated VIIRS Proxy	10	Yes	Dual gain	Same as (2) above with simulated fires added on top of real scenes	Control detailed characteristics of fires on top of real backgrounds
4	Full VIIRS simulation	16	Yes	Dual gain	Real or simulated VIIRS data with actual geometry	To be performed when simulated or real VIIRS data is available

4.2. Testing with Real MODIS Data

This approach was used to verify proper implementation of the fire mask by direct comparison of our implementation to the MODIS Version 4 output for identical scenes. This test was performed for the three scenes described in Section 4.3 and identical results where observed with both.

4.3. Testing with Real Fires Using VIIRS Proxy Mode

Testing based on real fires is used to examine the operation of the detection algorithm under different conditions. For this exercise, VIIRS proxy scenes were generated which differ from the original MODIS data in three ways. First, SDR values within the bowtie overlap region are filled with null values to represent the effects of modified bowtie deletion. Second, the low- and high-gain MWIR bands of MODIS have been combined into a single dual gain band. Third, VIIRS saturation thresholds have been applied to the MWIR and LWIR bands (T13 and T15). On the other hand, no adjustment is made for the differences in bandpass and more significantly, the differences in spatial resolution. These latter aspects are included in the performance analyses based on simulated data of the next section. We note that the smaller pixel size will increase the probability of fire detection (as a fixed fire size is a larger fraction of a pixel).

Figure 10 – The fire mask generated from the VIIRS proxy data includes the effects of bowtie deletion as illustrated for a portion of the Canadian forest fire scene (183.1900). In this representation, water is blue, clouds are white, non-fire pixels are green, and fire pixels are red (barely visible in the center of the image).

Three scenes are discussed in this section. The first corresponds to a region of forest fires in central Canada (183.1900). The second scene (187.1835) is from the western US and includes the Aspen fire.

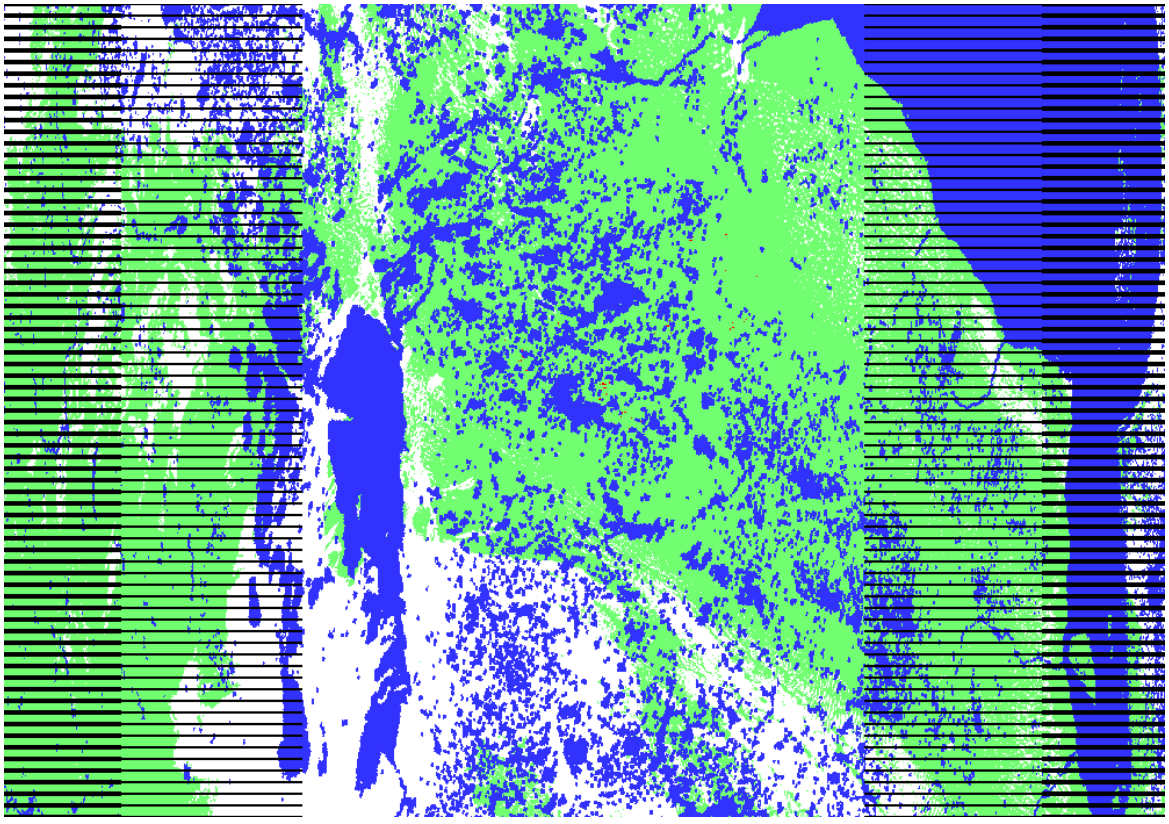

The third scene (183.1420) addresses agricultural burning in South America. The performance of the fire detection is evaluated by visual inspection of the fire mask relative to the input brightness temperatures and reflectances. Figure 10 shows a portion of the cloud mask from the central Canada scene which includes the pattern resulting from the bowtie deletion (dark stripes).

A region of active fires from the Canada scene (183.1900) is illustrated in Figure 11. In this case, the fire mask was generated using internal cloud tests (left) and using the MODIS cloud mask (right).

Clearly, the mask based on internal cloud tests performs better in this instance. In this case, all hot spots are detected as fire except for those that are misidentified as water due to inaccuracies in the land-water mask. The extended regions of smoldering fires are also not so easily identified. Figure 12 is a plot of the T13 brightness temperature and T13-T15 brightness temperature difference for the Canada forest fire scene. This plot illustrates the threshold for potential fires relative to the signal from all pixels in the scene and the classification of all potential fires plotted as a function of the same parameters. A few pixels are not identified as potential fires because the reflectance R5 exceeds the threshold of 0.30.

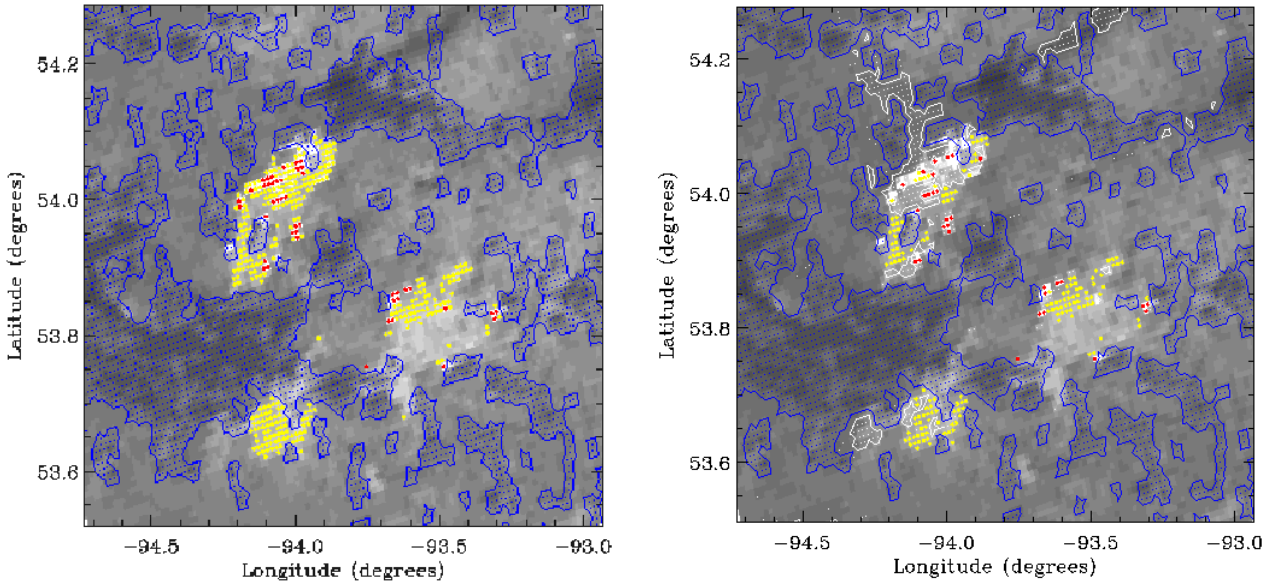

Figure 11 – Potential (yellow) and detected fires (red) are superimposed on a map of T13 brightness temperature for a region in Manitoba (183.1900). The results on the left were generated using the internal cloud tests. The results on the right were generated using the MODIS cloud mask. In the latter case, the identification of pixels as cloud results in numerous missed detections. Hot spots are detected but large smoldering areas are not. Also errors in the water mask result in several missed detection.

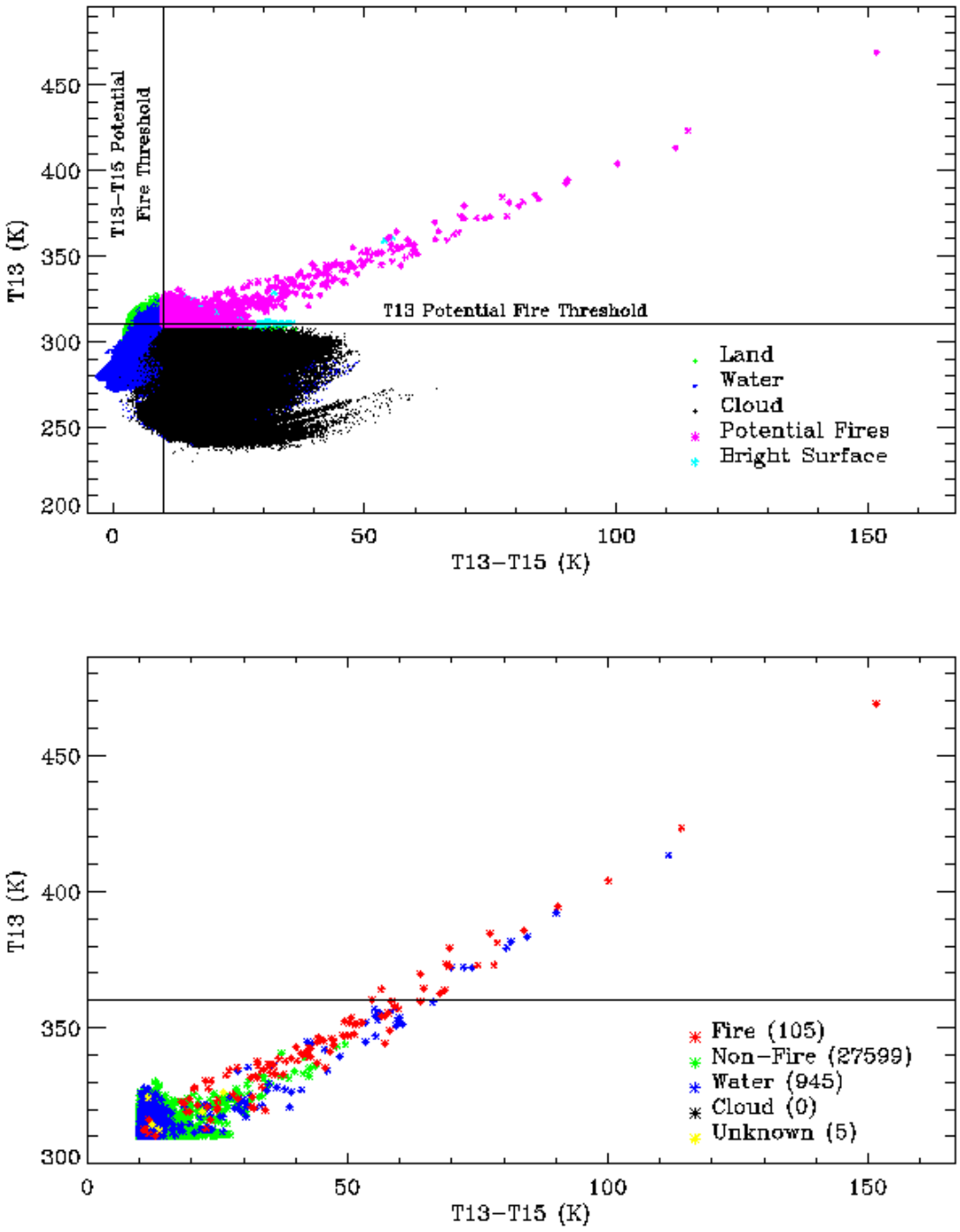

Figure 12 – The top plot shows all T13 brightness temperatures and T13 – T15 brightness temperature differences for MODIS granule 183.1900 (Canada forest fires). Potential fires are identified based on the thresholds T13>310, T13-T15>10, and R2<0.3. Pixels with T13>310 and T13-T15>10 but R2>0.3 are identified as bright surfaces and are not processed by the fire detection algorithm. The bottom plot shows the classifications (fire, non-fire, water, cloud, unknown) determined by the fire detection algorithm for all potential fire pixels and the absolute fire test T13 > 360 for day time conditions.

Analysis of the Western US (187.1835) and Brazil (183.1420) are presented in Figure 13 and Figure 14.

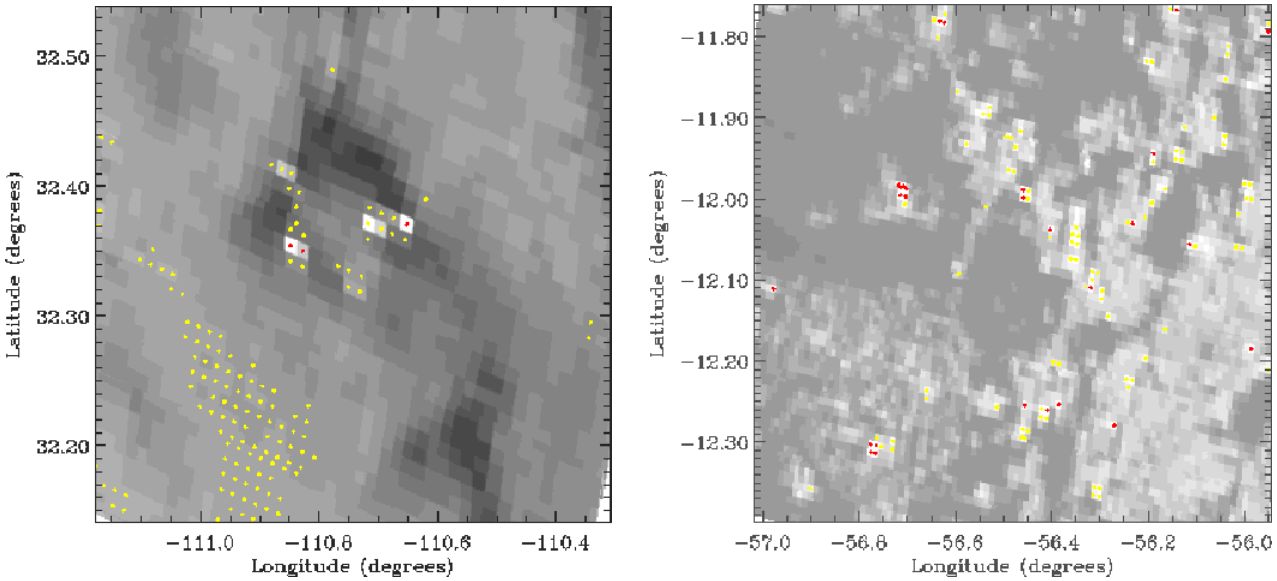

Figure 13 – The Aspen fire in Arizona from the Western US scene (187.1835) is shown on the left. Agricultural fires in Brazil (183.1420) are shown on the right. These maps show potential (yellow) and detected (red) fires superimposed on a MWIR image.

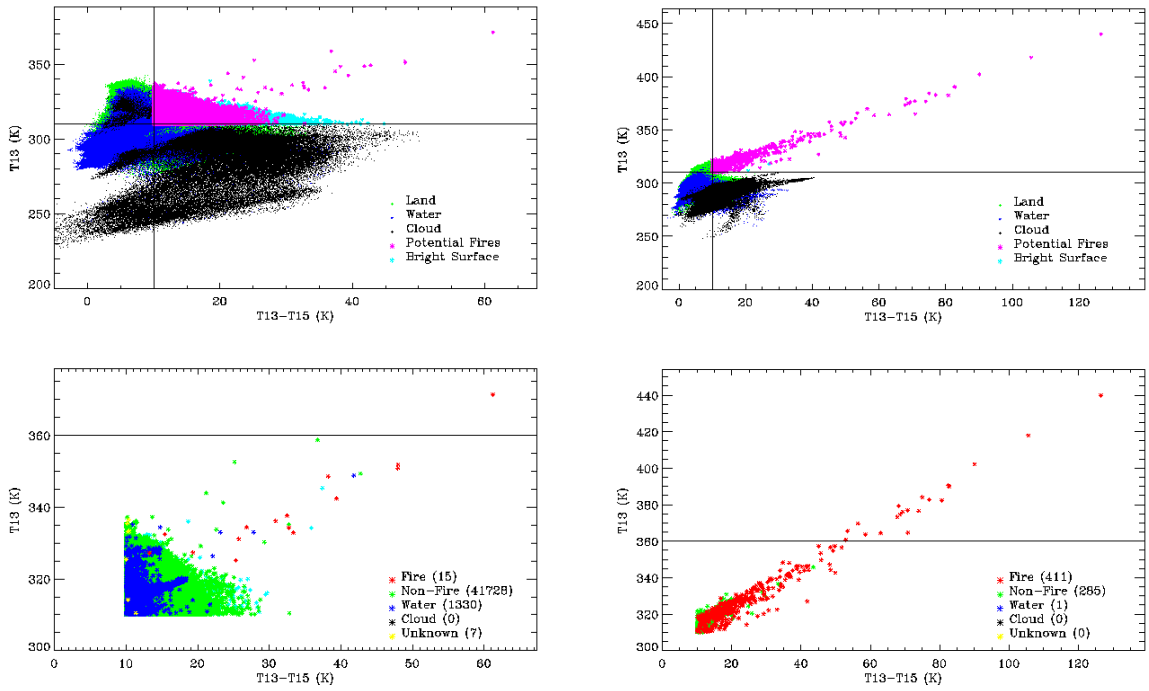

Figure 14 – Same as Figure 12 but for Western US scene (187.1835) left and Brazil scene (183.1420) right.

4.4. Testing with Simulated Fires

The performance of the VIIRS fire detection was then evaluated using simulated fires that were introduced into a scene based on real data. The source for the underlying background scene was MODIS. The use of the MODIS scenes ensures that the background clutter has realistic characteristics. This is important since the contextual fire tests are very sensitive to the clutter statistics.

Fire patterns were generated using a model that takes into account the flaming, smoldering, and background contributions to the signal. The approach is adapted from the fire simulation method used in Shephard and Kennelly (2003). The fire characteristics for the flaming and smoldering elements for the various fire types were taken from the description of natural fire morphology contained in Lobert and Warnatz (1993). These fire patterns were used as templates to place fires of varied types at multiple locations in a given MODIS scene.

The overall process is illustrated in Figure 15.

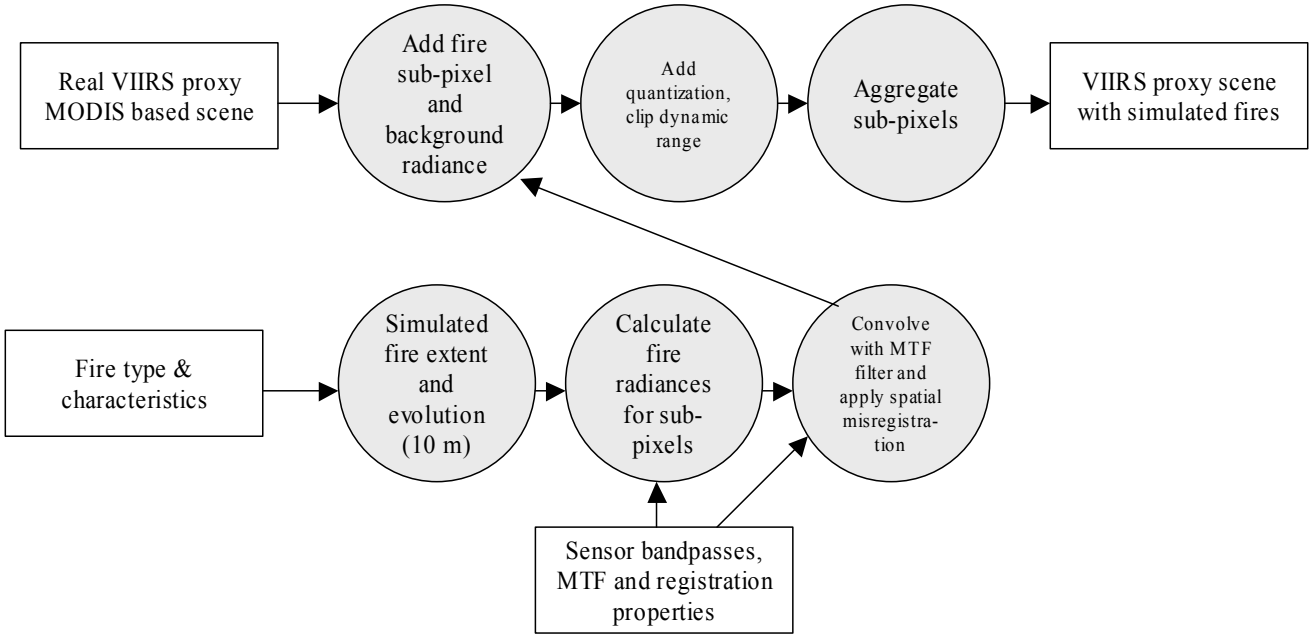

Figure 15 – Simulated fire scene generation process

The fire templates were generated at 10 m resolution and then convolved with the VIIRS instrument spatial response. For this study, the response functions of the sub-pixels (before aggregation) are assumed to be triangular in the scan direction and rectangular in the track direction. To represent the performance over the complete range of the VIIRS scan, we simulated the response at three scan angles (nadir, middle of scan, and edge of scan). For these cases, the FWHM of the response was 0.26 by 0.74 km, 0.52 by 1.0 km, and 1.6 by 1.6 km. Three fire patterns were created. The "multi"-fire template consists of several small fires located within a 10 km by 10 km area. The "ring"-fire template consists of a single ring of fire with smoldering pixels located within the perimeter. The "big"-fire template is similar to the ring but extends over a larger area (approximately 8 km).

The fire templates are shown in Figure 16. Note that it is possible for a fire (oriented along track) to fill most of a nadir sub-pixel, resulting in saturation of the MWIR sub-pixel if the temperature of the fire is larger than the saturation limit.

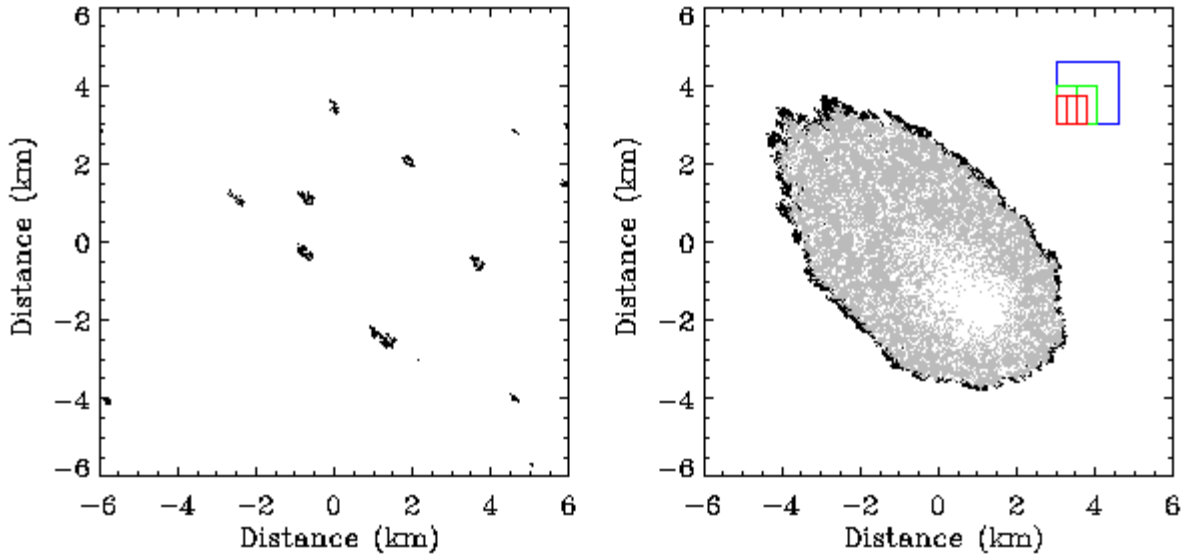

Figure 16 – Fire templates were generated at 10 m resolution. This plot shows the "multi-"fire (left) and "big"-fire (right) templates. Black, gray, and white areas represent the flaming, smoldering, and background components respectively. A typical scale of the fire front is 50 m. The right-hand plot shows the scale of sub-pixel resolution at nadir (red), middle-of-scan (green), and end-of-scan (blue).

The simulated fires were added randomly to scenes in regions that were not associated with water, cloud, or any existing real fires. The Brazil (183.1420), Western US (187.1835), and nighttime Central Canada (183.3045) scenes were used for the study. Depending on the location in the scene, fire templates convolved with the nadir, middle-of-scan, or end-of-scan response were used. If the fire was located in the nadir region then the fire template was sampled and binned to represent the VIIRS 3 pixel aggregation. If the fire was located in the middle-of-scan region, then the fire template was sampled and binned to represent 2 pixel aggregation. In the end-of-scan region the fire template was sampled but not binned, consistent with no aggregation. The positioning of the fires in the scene took bowtie overlap into account. Each fire was assigned a random fire temperature ranging from 400 to 1200 K. The temperature in the smoldering region was limited to half that of the flaming portion. The temperature of the background was derived from the brightness temperatures of the original uncontaminated pixels. Radiances in the MWIR and LWIR bands were computed for the three components (i.e., flaming, smoldering and background), weighted by the corresponding fractions, and summed. These signals were converted to counts, and then saturation limits and quantization were applied. The signal in the NIR band was simulated by computing the weighted sum of the original background signal with the signal from the fire and smoldering region (assumed to have a reflectance of 0.1).

Fires based on the 'multi'-fire and 'ring'-fire templates were added to the Brazil scene. Fires based on the 'multi'-fire, 'ring'-fire, and 'big'-fire templates were added to the Western US scene. Fires based on the 'multi'-fire and 'big'-fire templates were added to the Central Canada scene. The VIIRS fire detection algorithm was applied to each of these scenes and the performance of the retrievals was

expressed in terms of the probability of detection. Real fires associated with the original scene were eliminated from the statistics.

Figure 17 illustrates the product of the simulations. Figure 18 illustrates the results of the fire detection on the Brazil 'multi'-fire scene.

Figure 17 – The left MWIR brightness temperature image shows the portion of the Brazil scene where fires have been added based on the 'multi'-fire template. The right MWIR image shows a portion of the Western US scenes where fires have been added based on the 'big'-fire template.

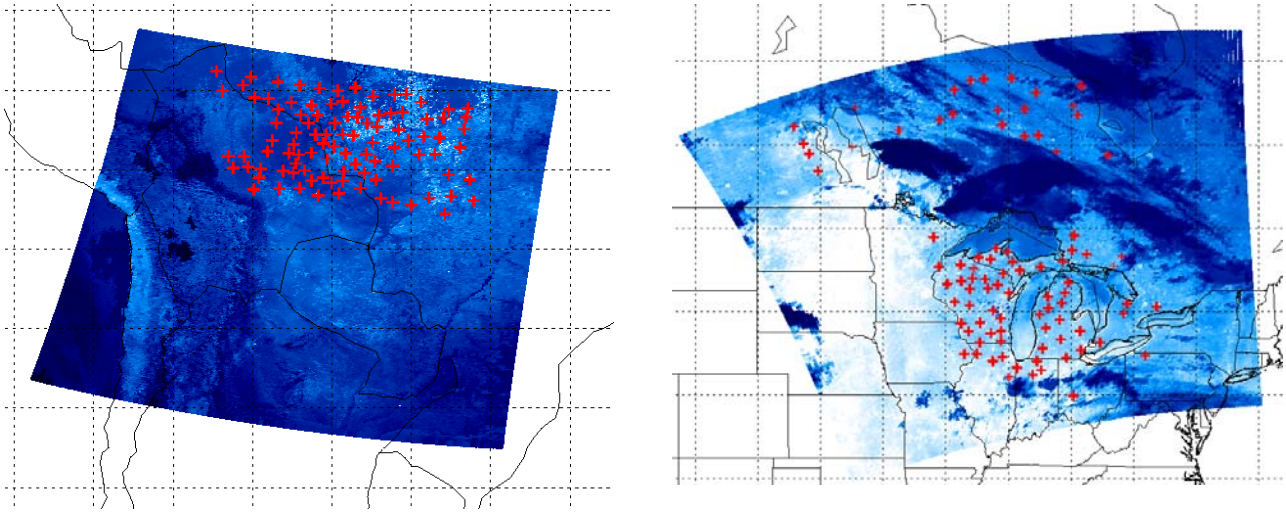

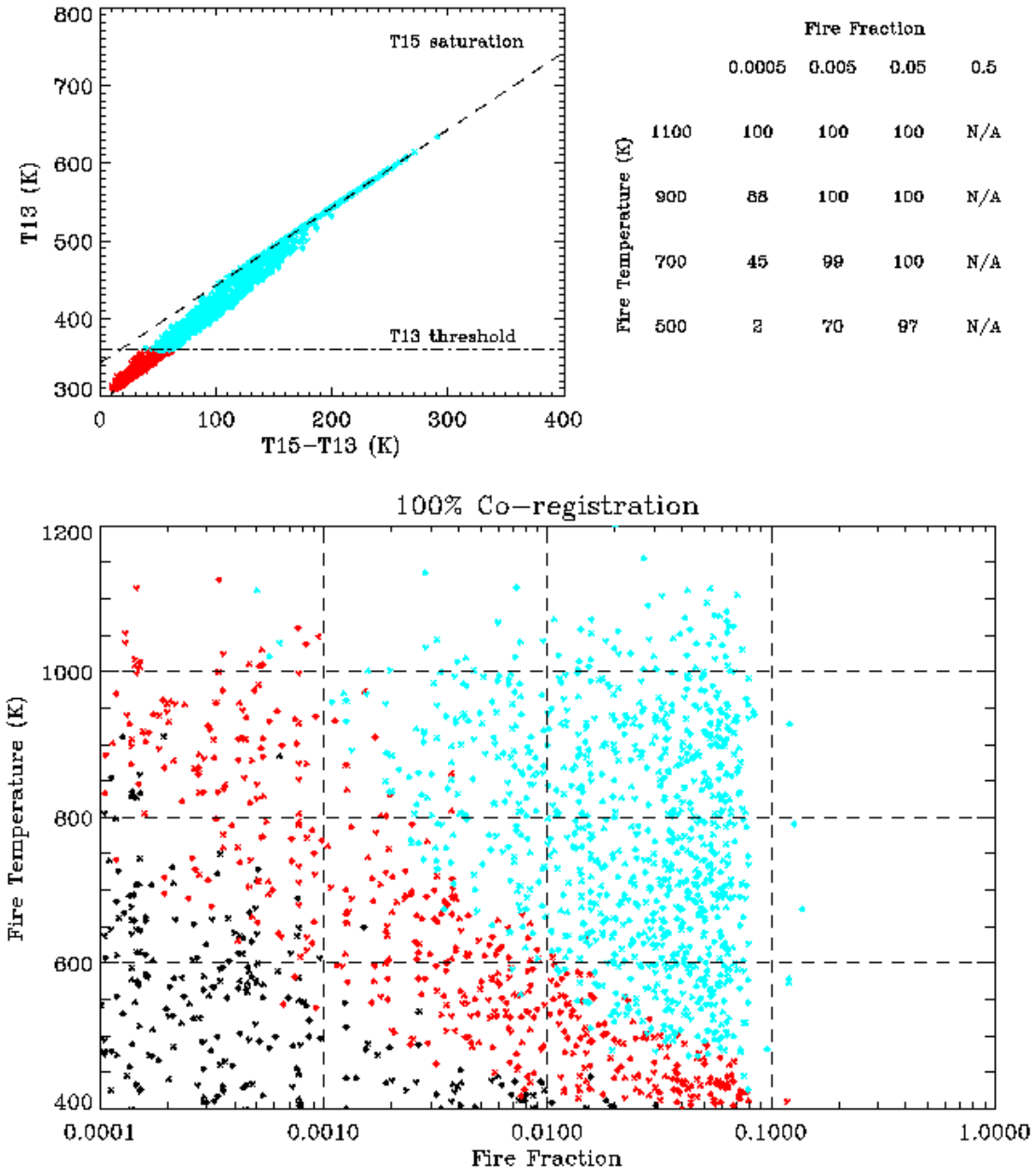

Figure 18 – Nominal performance based on multi-fire simulation in Brazil. The top left plot shows the detected fires as a function of the MWIR brightness temperature and MWIR-LWIR brightness temperature difference. The threshold for absolute fire detection based on the MWIR band is indicated (at 360 K) as is the line corresponding to saturation in the LWIR band (at 343 K). The table on the top right gives the probability of detection for sixteen bins as a function of fire temperature and fire fraction. At the bottom is a scatter plot of all simulated non-detected (black) and detected (red) fires with fractions greater than 0.0001.

The impact of band-to-band co-registration was evaluated using the MODIS-based simulation methodology. For this part of the study, mis-registration errors of 70, 80, 85, and 90% of the pixel size in each dimension were introduced in to the LWIR band relative to the MWIR band before sampling to the VIIRS resolution. Specified in this manner, mis-registration of 80% corresponds to the VIIRS co-registration specification for these bands.

Figure 19 shows an example of the results. Figure 20 summarizes the results of the co-registration study in terms of the detection probability. The VIIRS fire detection algorithm performs very well over most temperatures and fire fractions.

Only for very small/cool fires are any differences in detection noted. Also, the impact of mis-registration clearly has very little impact on the overall performance statistics

4.5. Summary of testing

Table 11 summarizes the type and number of tests performed.

Table 11 – Summary of tests performed on cloud mask

Scene	Real data testing	Day/ Night	Simulated fires added			Registration offsets	Clouds	Saturation	Fire locations
			"Big"	"Multi"	"Ring"				
Arizona	x	Day		x	x	6 offsets from 0 to 200%	Scenes contain varied cloud types	VIIRS saturation specs & unsaturated	Fires placed nadir, mid and near edge of scan
Manitoba	x	Night	x	x					
Brazil	x	Day		x	x				

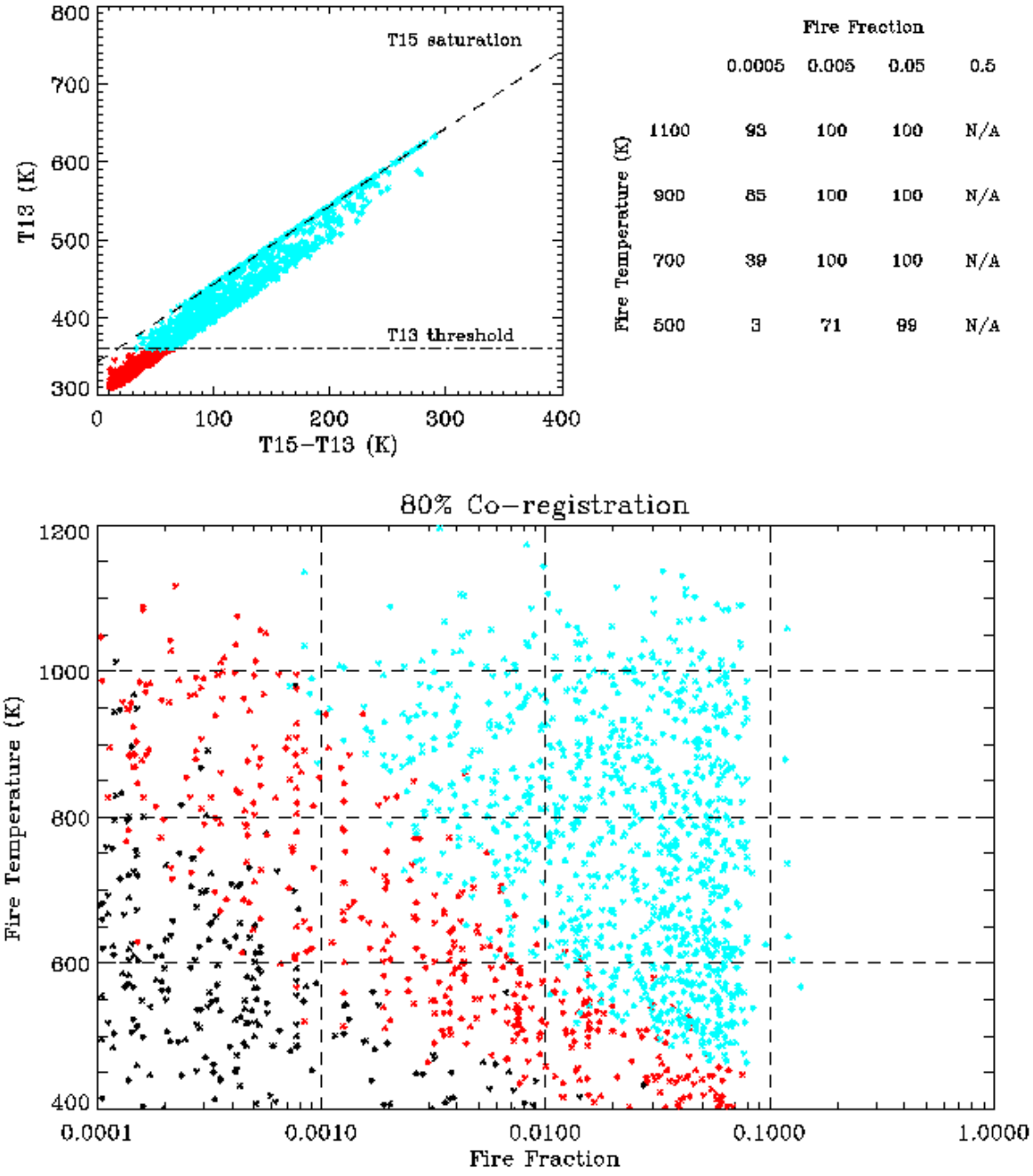

Figure 19 – This figure includes a mis-registration of the LWIR and MWIR bands of 80%. In the increased spread in MWIR-LWIR brightness temperature difference due to mis-registration is clearly visible. A few fires with MWIR temperatures below the 360 K threshold and with small temperature differences go undetected (indicated by the black symbols).

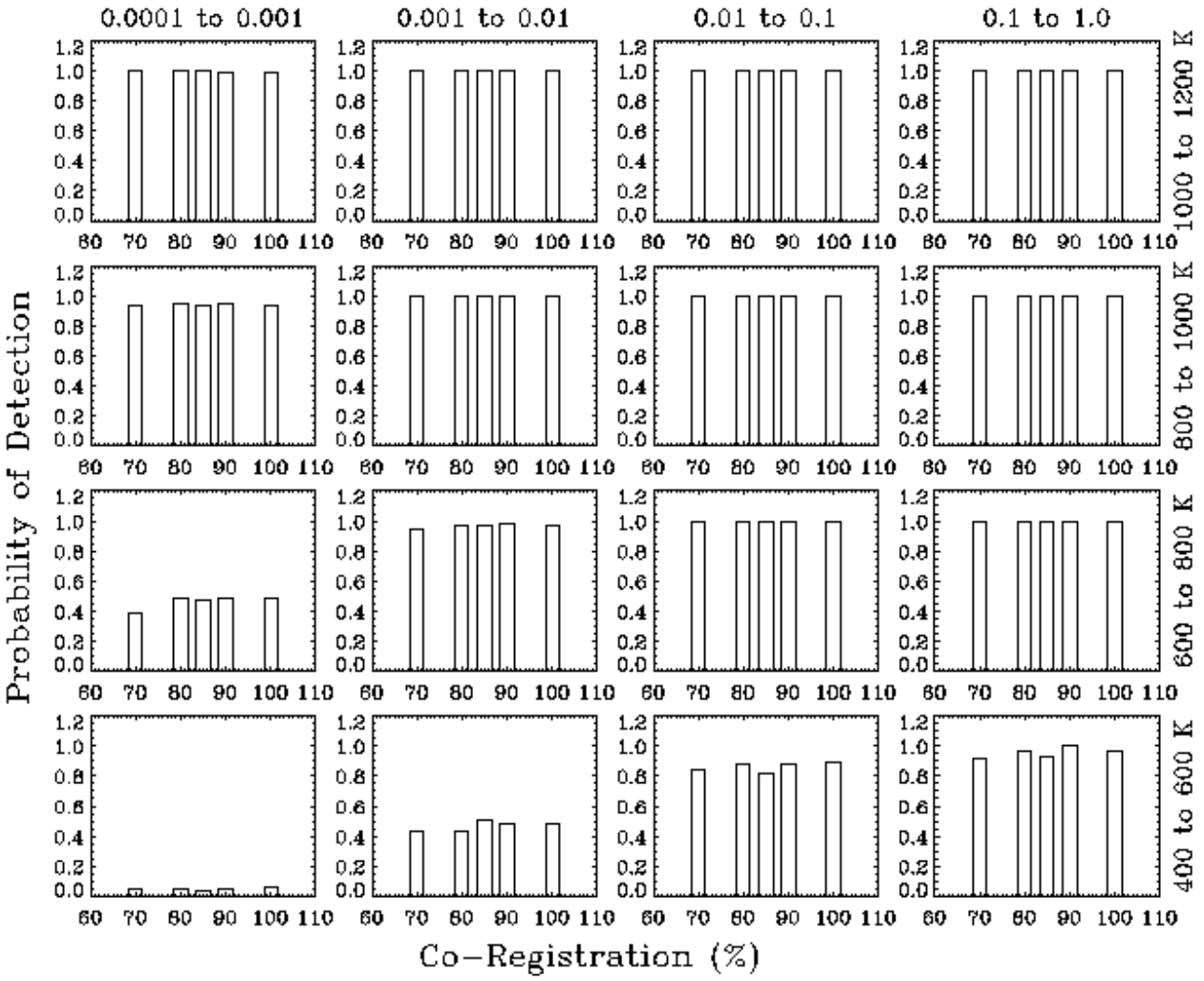

Figure 20 – Co-registration has minimal impact on VIIRS fire detection. This plot shows the probability of detection as a function of MWIR-LWIR co-registration for fires divided into sixteen temperature (right hand side vertical axis) and fraction bins (top horizontal axis). Large hot fires which are detected with the MWIR band alone are not impacted by co-registration errors. Small cooler fires which are detected via contextual tests may be affected but the overall impact is not much larger than the statistical variations in the study itself.

4.6. Algorithm Performance Assessment

This section summarizes performance assessment in the critical categories.

Impact of MWIR Saturation – Saturation of the MWIR band has no impact on VIIRS fire detection. This is clearly illustrated in Figure 21 which demonstrates that if a single sub-pixel saturates, the resulting signal will always exceed the level required for absolute detection of the fires based on the MWIR channel alone.

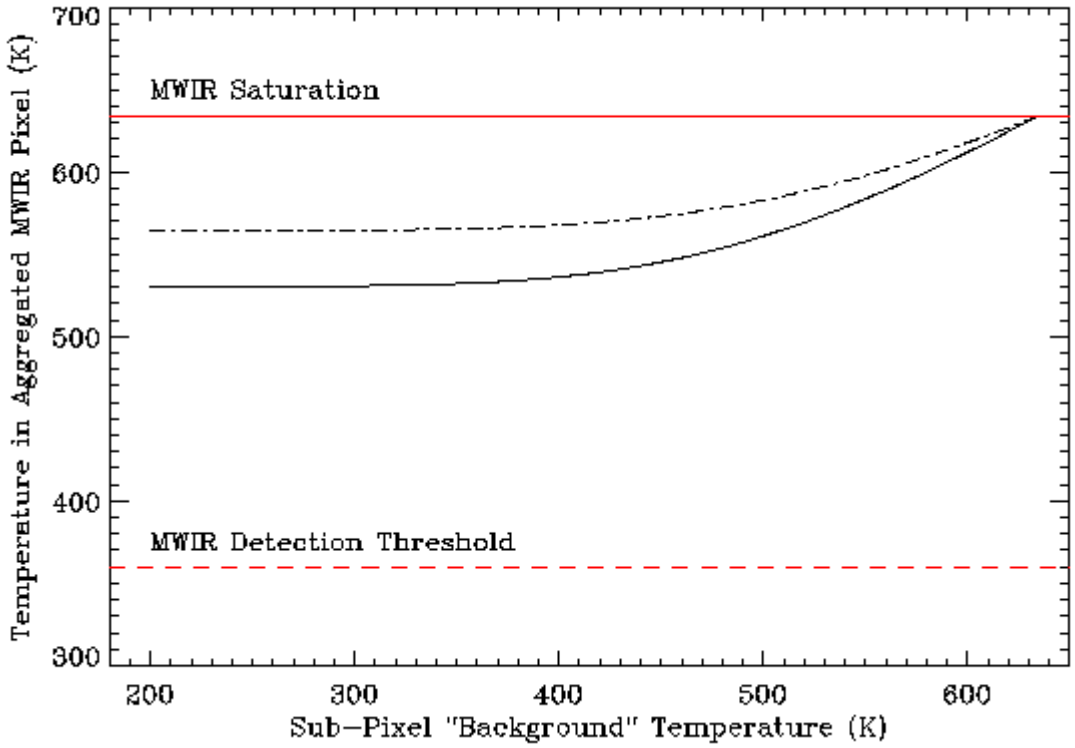

Figure 21 Saturation of MWIR sub-pixels has no impact on the detection of fires. This plot shows the brightness temperature in the aggregated nadir (solid black) and middle-of-scan (dashed black) pixels when one sub-pixel saturates (at 634 K), as a function of the temperature in the remaining sub-pixel aggregates. Even if the signal in the neighboring sub-pixels is very cold (e.g., cloud), the combined signal will still exceed the MWIR detection threshold.

Impact of LWIR Saturation – The impact of saturation in the LWIR Band (M15) was examined in Figure 7. This figure showed that only a very small region of the fire state space (in particular large, lower temperature fires) use tests that could potentially be affected by LWIR channel saturation. This region is well outside the fire measurement range given in the NPOESS specification and consists of temperatures more characteristic of smoldering conditions than an active fire – thus questioning whether such pixels are reasonably classified as fire.

Few fires are observed in this region. Figure 22 is typical where none of the pixels has fire characteristics in the sensitive region.

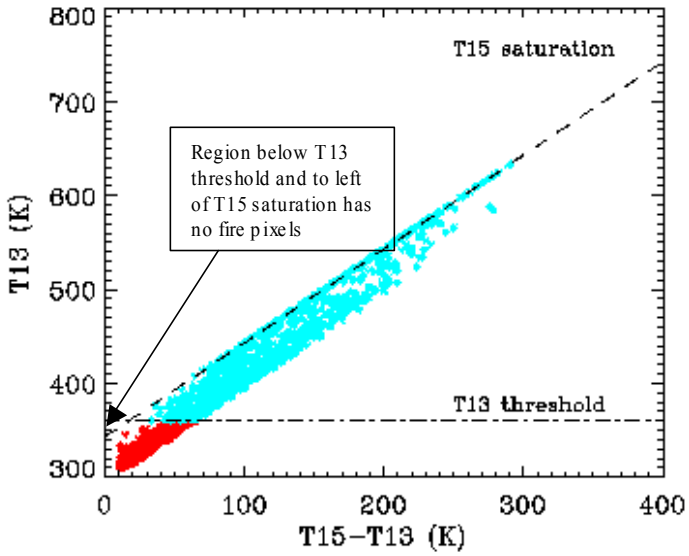

Figure 22 – Region where fire tests are potentially affected by M15 saturation is not populated by any fires

While this region is not populated with active fires, there are smoldering areas that exist in this region. These regions will affect the contextual search and thus indirectly may influence which pixels are classified as fire. There are also small effects on the prescreening portion of the algorithm.

To test this we took the three simulated fire scenes (one day, two night) used above and ran them in two ways: once using the standard band M15 saturation of 343 K and once with no saturation but all other parameters the same. We term these the nominal VIIRS and non-saturating VIIRS cases, respectively. The "multi-fire" fire type was chosen for the fire template as it is very stressing (many small fires, high dependence on contextual search).

Figure 23 shows the results of this test. The results are summarized in Table 12. The three scenes have a total of 13,525 total input fires, many below the threshold of detectability. Nominal VIIRS detects 3,413 fires, slightly more than the non-saturating VIIRS case. This is as expected: the effect of saturation is to increase slightly the local variability and thus increase the number of fires flagged. The net difference in the number of fires is small (~1.6%). In terms of specific fires flagged, a total of 7.7% are flagged in nominal VIIRS but not the non-saturating case. The converse case has 7.1%. These differences are mostly due to the contextual test and relate to fires near the threshold of detection.

Table 12 – Summary comparison of Nominal VIIRS and non-saturating VIIRS fire detection comparison

Simulation	Total # Fires detected	# Detected in the simulation, but excluded in other (#/%)			
		Over all detected fires			Fires within measurement range
		Contextual	Test 1	Total	Total for fires within specified range
Nominal VIIRS	3,413	171/ 5.0%	75/ 2.2%	75/ 2.2%	25/ 0.7%
Non-saturating VIIRS	3,358	46/ 4.3%	61/ 1.8%	61/ 1.8%	28/ 0.8%
Difference (#/%)	55/ 1.6%				

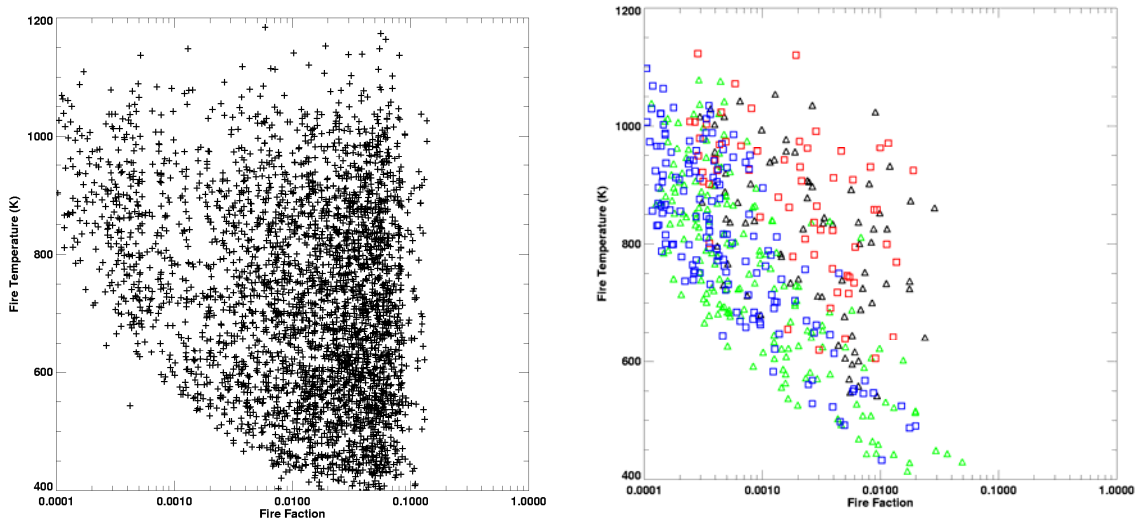

Figure 23 -- Comparison of "nominal VIIRS" to "non-saturating VIIRS" fire detection using simulated VIIRS test approach. Left shows all fires detected by the control case: nominal VIIRS. Right indicates fires detected in one simulation but not the other. Black triangles: nominal VIIRS, test 1; Green triangles: nominal VIIRS, contextual tests; Red squares: non-saturating VIIRS, test 1; Blue squares: non-saturating VIIRS, contextual tests

The difference for fires within the required measurement range (≥ 800K and f≥ 0.001) is much smaller. The number of pixels detected in one case, but not in the other is < 1%.

In conclusion, some differences are noted in the fire detection between cases of VIIRS with and without a saturating 10.6 μm channel. When restricted to fire pixels within the specified measurement range, the differences are very small (< 1%). Some of the differences result from the fact that in a heterogeneous scene (not at the edge of scan where no aggregation occurs) it is not possible to unambiguously identify which M15 band pixels are saturated (see Section 3.4.1). If such

flagging could be added (likely requiring some change in the onboard VIIRS signal processing), then additional improvement could likely be obtained.

Impact of Band-to-Band Mis-Registration – The analysis presented in Section 4.4 (see Figure 20) demonstrated that fire detection with VIIRS is affected very little by mis-registration of the MWIR and LWIR bands. The reason for this is that with the smaller footprint provided by VIIRS (compared to MODIS), a larger number of fires are detected based on the absolute threshold on the MWIR band. Small/cool fires which do not produce signals that exceed the MWIR threshold are detected based on contextual tests that rely, in part, on the difference in MWIR and LWIR brightness temperatures. In some instances, errors in band co-registration will decrease the T13-T15 brightness temperature difference (i.e., increase T15) below the threshold required for fire detection (Fire Detection Test #2 and #3). This will only occur when signal adjacent to the MWIR pixel is hotter than the true LWIR temperature (e.g., due to a bigger/hotter fire). In this case, even if the detection of the fire is missed, it is likely that that the adjacent fire will not go undetected. In other instances, the brightness temperature in the LWIR band will be decreased relative to the true signal causing Fire Detection Test #5 to fail. However, this test is only important if Fire Detection Test #6 (which identifies highly variable MWIR background with the presence of large fires) also fails.

On the other hand, co-registration errors could cause fires to be detected in locations that would not otherwise pass the detection criteria if the bands were perfectly co-registered. This is likely an infrequent occurrence producing very few false alarms. This effect has not been studied in this report but could be evaluated using a source of high-resolution MWIR/LWIR scenes with realistic background variability.

Errors due to Sun Glint – The VIIRS fire detection algorithm leverages the experience from operational MODIS retrievals to address possible errors resulting from sun glint. Thus the false alarm rate due to sunglint is expected to be acceptably low. The sun glint rejection routine described in the VIIRS algorithm uses the MODIS thresholds. Only minor tuning may be required to account for bandpass differences. Scenes (either observed or simulated) that include sun glint could be used to investigate sensitivities and tune the rejection parameters.

Errors due to Bright Surfaces – Bright surface exclusion is introduced via the near-IR potential fire test ($R7 < 0.30$). In many instances the presence of a fire is associated with a more extended burnt area which will cause this test to be satisfied. However, instances of new fires in areas of bright vegetation may cause fires to go undetected. The near-IR threshold is chosen to minimize the occurrence of false alarms caused by bright surfaces. Our testing and experience with MODIS indicates this is not a significant source of error.

Errors due to Land/Water – Inaccuracies in the land/water mask can be a problem for the fire detection algorithm. The example presented in Section 4.2 illustrated how fires can go undetected in Canada where a large fraction of the land area is covered by small water bodies which are not properly identified. In that case valid land pixels were identified as water. Errors in the water mask could also lead to false alarms if the water pixels are incorrectly identified as land by the mask. To reduce the occurrence of false detections introduced in this way, the fire detection algorithm includes a test for water based on NDVI and the R7 and R11 reflectances. This problem will be largely resolved when improved land/water masks are developed (e.g., by MODIS). We expect this contribution to be significantly reduced for NPOESS.

Errors due to Clouds – The identification of pixels as clouds circumvents fire detection. In many instances clouds may be present but the signal from the fire may be easily detected (e.g., for cirrus clouds). It is therefore important to identify clouds in a way that will not impact the detection of fires. In Section 4.3, the impact of the MODIS cloud mask on the fire product was illustrated.

It is expected that the standard VIIRS cloud mask would produce similar results because of its close relationship to the MODIS cloud mask. While the VIIRS fire detection algorithm includes an internal cloud detection algorithm, we believe ultimately it is preferable to use the VIIRS cloud mask. To perform adequately it will almost certainly be required to derive the fire mask cloud mask from a selected subset of the VIIRS tests perhaps with adjusted thresholds.

At the time when this development was done, the VIIRS cloud mask was not available for integration with the fire algorithm. However, this could be accomplished as part of integration testing of the entire VIIRS algorithm suite. Since the delivered algorithm code is configured to use either the internal cloud mask or an external mask, such testing is easily performed.

Instances of possible false alarm due to missed cloud detection have not been quantified with the present algorithm. Manual inspection of the test scenes indicates that this is not a significant problem.

Correction for the presence of clouds are expected to have negligible benefit for the detection of fires based either on the absolute MWIR thresholds or based on contextual tests relative to the surrounding background.

Impact of Atmospheric Absorption – Atmospheric absorption in the MWIR band is small and has negligible impact on the detection of fires via the MWIR absolute threshold test. The effects of atmospheric absorption in the LWIR band are reduced by the use of this band for contextual tests only.

Impact of Solar Contamination – The impact of solar contamination in the MWIR band on the VIIRS fire detection product has not been investigated in this report. The impact is expected to be small. Further testing based on radiative transfer simulations could be conducted to determine the magnitude of the solar effects on fire detection.

Detection and False Alarm Probabilities – In Section 4.4, fire detection probabilities for the VIIRS sensor design were evaluated based on one methodology for creating simulations. Fires with signals consistent with the VIIRS sensor design were added to background scenes derived from MODIS observations. The results indicate that the VIIRS detection algorithm will perform very well, with close to 100% detection for most of the parameter range investigated. Compared to current sensors (e.g., MODIS), the VIIRS instrument is expected to produce a much improved fire detection product. This is largely due to the improved spatial resolution. It is anticipated that the VIIRS false alarm probabilities will be similar to MODIS which has been optimized to minimize the number of false detections. False alarm probabilities were not addressed in the MODIS-based simulations due to the difficulty in identifying the validity of the detections in the underlying background scene.

Other testing methodologies are required to evaluate the VIIRS false alarm statistics. In particular the planned simulation to be performed by the NGST Modeling and Simulation Team will be able to derive these statistics.

Algorithm Tuning – The VIIRS fire detection algorithm has been designed with all tunable parameters included in a configuration file. This feature of the algorithm makes possible sensitivities studies and the further optimization of the fire detection parameters based on a set of representative VIIRS scenes. This permits algorithm testing to continue in parallel with the software development as changes to thresholds need only update the configuration files. To date, our testing has not revealed any need to change the threshold values from the MODIS settings.

4.7. Probability of detection error budget

The VIIRS simulation includes most of the significant effects contributing to the probability of correctly detecting a fire. The error budget of Table 13 below combines the output of these simulations with estimates of the other parameters discussed above.

Table 13 – Error budget for probability of correctly detecting a fire for limiting fire case within specified measurement range

Type	Error component	Edge of scan	Nadir	Method
Probability of not detecting a fire within specified measurement range, P-nf	Basic fire detection from simulation which includes sensor noise, MTF, saturation, co-registration and intrinsic algorithm errors	5.0%	2.0%	Detailed simulation
	Bright surface	0.50%	0.50%	Estimate
	Land/ water mask	0.50%	0.50%	Estimate
	Cloud	1.00%	1.00%	Estimate
	Atmospheric absorption	0.50%	0.50%	Estimate
	Solar contamination	0.50%	0.50%	Estimate
	Root sum square of above	5.2%	1.7%	
	Margin	2.0%	2.0%	
Probability of correctly detecting a fire, Pf (100% - P-nf)		92.8%	96.3%	

5. Practical Considerations

5.1. Numerical Computing Considerations

The VFM employs simple tests and does not employ any numerically complex or unstable algorithms. No special precautions are expected to be required to maintain numerical accuracy.

While the algorithm has not been bench-marked for processing throughput, it has not been observed to present high CPU demand.

5.2. Programming Considerations

The algorithm is coded in ANSI C/C++. Interfaces to sensor and other data are through an object oriented standard application programmer's interface (API) and should be able to be easily adapted to the target environment. See the software documentation for additional details on the software design.

5.3. Computer Hardware/ Software Requirements

While the algorithm has not been bench-marked for processing timing/ resource requirements, it has not been observed to present high CPU demands. Also the fire mask is dependent only on the SDR data as input (although in the future it may also require the cloud mask). The only algorithm dependent on its output is the fire temperature/ area algorithm. This latter algorithm is only applied to the small fraction of pixels identified as fire. Thus, we do not anticipate it being an IDPS processing driver.

A description of the software and computer environmental requirements is included in VIIRS Active Fires: Fire Mask – Software Documentation (P1187-SW-I-001).

5.4. Quality Control and Diagnostics

In addition to a fire/ no fire flag, the VFM outputs a detailed mask containing information on the various tests and thresholds. This mask will be important for final algorithm tuning and algorithm debugging. Minimally this quality control mask should be made available to support Cal/ Val, periodic algorithm spot tuning and algorithm problem resolution.

5.5. Exception and Error Handling

The software checks for bad, missing pixels (denoted by a fill value) and missing ancillary data. It does not perform a retrieval in such cases.

5.6. Special Database Requirements

The algorithm requires a high quality land-water mask as input. The current algorithm obtains this via the ancillary data input file. The current version of the land/ water mask has poor quality in some inland regions with many small lakes. It would be desirable to employ an improved mask when one becomes available. We note this requirement pertains to other NPOESS EDRs.

5.7. Archival Requirements

The Fire Mask algorithm provides three outputs described in Table 6. We recommend the following archiving:

- Fire_Mask: Archive all output per NPOESS requirements
- Fire_QC: Archive all output per NPOESS requirements
- Fire_Diagnostics: At a minimum, archive data to support Cal/Val operations and as required for algorithm tuning, and trouble shooting. Additional archiving subject to discussion with Science Team.

6. List of References

Dozier, J. (1981). A method for satellite identification of surface temperature fields of subpixel resolution, *Remote Sensing of Environment*, 11, 221-229.

Giglio, Louis, Jacques Descloitres, Christopher Justice, and Yoram Kaufman (2003): An enhanced contextual fire detection algorithm for MODIS, submitted to Remote Sensing of Environment.

Giglio, L., and J. D. Kendall (2000). Application of the Dozier retrieval to wildfire characterization: a sensitivity analysis. Submitted to *Remote Sensing of Environment*.

Justice, Christopher (2002): MODIS Fire Validation and Status Report and Rapid Response Update, from MODIS Science Team Meeting - Plenary Session Presentations, July 24, 2002 (http://modis.gsfc.nasa.gov/sci_team/meetings/200207/pres_jul2002wed.html).

Kaufman, Y., and C. Justice, 1998: *MODIS Fire Products Algorithm Technical Background Document*, Version 2.2, EOS ID #2741.

Lobert, J. M. and J. Warnatz, 1993: Emissions from the Combustion Process of Vegetation, appearing in Fire in the Environment: The Ecological, Atmospheric and Climate Importance of Vegetation Fires, J. Wiley and Sons. P. Crutzen and J. G. Goldhammer, ed., pp 15-38.

Miller, S. and Q. Liu, 2002: VIIRS Active Fires Algorithm Theoretical Basis Document (ATBD), Version 5, Raytheon ITSS.

Shephard, Mark, L. Giglio and J. Kendall, 2000: VIIRS ATBD for the Active Fires EDR, Version 1.4, May 2000, AER, Inc.

Shephard, M. W. and E. J. Kennelly, 2003: Effect of Band-to-Band Co-registration on Fire Property Retrievals. I.E.E.E. Trans. Geoscience and Remote Sens., in press.

Visible/Infrared Imager Radiometer Suite (VIIRS), Active Fires: Fire Mask, Software Documentation 2003: Version 1.0.1, Document Number P1187-SW-I-001, Atmospheric Environmental Research, Inc.

Ted Kennelly, David Hogan and Scott Zaccheo, 2004: Visible Infrared Imaging Radiometer Suite (VIIRS) Determining Active Fires Characteristics for NPOESS, Trade Study Report, Atmospheric Environmental Research, Inc., Document Number P1187-TR-I-003.

Appendix A – Detailed Algorithm Comparison

The following table compares the features of the delivered VIIRS Version 6 algorithm with MODIS Version 4 and VIIRS Version 5.

References to T_4 refer to the 4 μm band brightness temperature (VIIRS Band M13, and MODIS 21/22). T_{11} refers to the 11 μm channel.

	MODIS (Version 4)	VIIRS (Raytheon, Version 5)	VIIRS (AER, Version 6)
Surface Test	Create water mask based on MODIS land/sea mask	Identify water, snow, ice, and urban based on quarterly surface type map	*Perform fire retrievals on all land pixels. Include flags for snow, ice, and urban.*
Cloud Test	Create cloud mask based on simple cloud algorithm, internal to algorithm	Identify clear/cloudy based on VIIRS cloud mask	*Analyze errors in fire retrievals due to VIIRS cloud mask (some tests in VIIRS cloud mask will incorrectly flag fires as cloud per MODIS experience)* *Baseline to use cloud tests internal to fire mask algorithm, configurable option uses external cloud mask*
Cirrus Cloud Test and Correction	N/A	Apply cirrus cloud correction based on cloud mask input. (Not Implemented)	*Omit this correction.*
Sun Glint Test	Rejected for potential sun glint if within 40 degrees of specular angle and surface is bright in nir band	Identify sun glint contamination based on VIIRS cloud mask input (within 31 degrees of specular angle), no retrieval in these cases regardless of whether the nir pixel is bright	*Use MODIS sun glint rejection criteria which will have much reduced sun glint outage*
NIR Test	N/A	Reject pixels if $\rho_{.86} > \rho_{max}$	*This test is included in potential fire test instead.*
Saturation Test	Replace M22 with M21 if saturated	Flag saturated pixels (need to review if test will work with actual VIIRS	*Algorithm to detect saturation may be required (need to review current*

		design and data formats) M13 dual gain covers full dynamic range and so no need to switch	*sensor behavior in saturating conditions with SBRS) – complicated by sub-pixel aggregation and A/D wrap-around and detector saturation*
Atmospheric Correction	N/A	Water vapor correction T_4 and T_{11} based on NCEP data (Not implemented)	*Impact on fire detection is small (Giglio). Omit this correction.*
Potential Fire Test	Daytime: Identify pixels with $T_4 > 310$, $\Delta T > 10$, and $\rho_{.86} < 0.30$ Nighttime: Identify pixels with $T_4 > 305$ and $\Delta T > 10$	Identify pixels with $T_4 > T_{min}$ and $\Delta T > \Delta T_{min}$	*Same as MODIS. May adjust thresholds based on subsequent testing.*
Absolute Fire Test	Daytime: Flag pixels with $T_4 > 360$ [1a] Nighttime: Flag pixels with $T_4 > 320$ [1b]	Flag pixels with $T_4 > T_{abs}$ [1]	*Same as MODIS. May adjust thresholds based on subsequent testing.*
Background fire test	Daytime: Identify pixels with $T_4 > 325$ and $\Delta T > 20$ Nighttime: Identify pixels with $T_4 > 310$ and $\Delta T > 10$	N/A	*Same as MODIS. May adjust thresholds based on subsequent testing..*
Background Statistics	Statistics are computed for all potential fires from surrounding valid background pixels. Compute mean (T_{4B} ,T_{11B} ,ΔT_B) and absolute mean deviation	Statistics are computed for all potential fires from all surrounding non-potential fires. Exclude pixels not of the same surface type. Compute mean (T_{4B} ,T_{11B} ,ΔT_B) and	*Adopt MODIS algorithm for background characterization.* *Modify nearest neighbor search algorithm for VIIRS configuration.*

	(δ_4 ,δ_{11} ,$\delta_{\Delta T}$) of valid background pixels. Compute mean T'_{4B} and absolute mean deviation δ'_{4B} of background fire pixels. Maximum box size is 21x21 pixels or when number of background pixels exceeds 25%. Optimized nearest neighbor search is used to locate background pixels taking bowtie overlap into account.	standard deviation (δ_4 ,δ_{11} ,$\delta_{\Delta T}$) of valid background pixels and background fire pixels (T'_{4B} ,T'_{11B} ,$\Delta T'_B$) standard deviation ($\delta_{\Im 4}$,$\delta_{\Im 11}$,$\delta_{\Im \Delta T}$) Maximum box size is 21x21 pixels or when number of background pixels exceeds 25% and is greater then or equal to 3.	
Contextual Tests	$\Delta T > \Delta T_B + 3.5\ \delta_{\Delta T}$ [2] $\Delta T > \Delta T_B + 6$ [3] $T_4 > T_{4B} + 3\ \delta_4$ [4] $T_{11} > T_{11B} + \delta_{11} - 4$ [5] $\delta'_4 > 5$ [6]	$T_4 > T_{4B} + 4\ \delta_4$ [2] $T_4 > T_{crit}$ [3] $\Delta T > \Delta T_B + 4\ \delta_{\Delta T}$ [4] $\Delta T > \Delta T_{crit}$ [5]	*Same as MODIS. May adjust thresholds based on subsequent testing.*
Fire Detection	Daytime: Flag pixels with [1] or [2]&[3]&[4]&([5] or [6]) Nighttime: Flag pixels with [1] or [2]&[3]&[4]	Flag pixels with [1] or ([2]or[3]) and ([4] or [5])	*Same as MODIS. May adjust thresholds based on subsequent testing.*
Sun Glint Rejection	Reject fires based on any one glint angle Θ_g criteria $\Theta_g < 2$ $\Theta_g < 8$ & $\rho_{.65} > 0.1$ & $\rho_{.86} > 0.2$	N/A	*Same as MODIS. May adjust thresholds based on subsequent testing.*

	& $\rho_{2.1} > 0.12$ $\Theta_g < 12$ & $(N_{aw} + N_w) > 0$ Where N_w is the number of water pixels in search box and N_{aw} is the number of water pixels within 8 pixels of candidate fire pixel		
Desert Boundary Rejection	Described in reference paper but not included in Version 4 algorithm. See Note A below.	N/A	*Not included.*
Coastal Rejection	Identify unmasked water pixels in search box where $\rho_{2.1} < 0.05$ & $\rho_{.86} < 0.15$ & NDVI < 0 Reject fires if the number of unmasked water pixels $N_{uw} > 0$ and absolute fire test is false.	N/A	*Same as MODIS. May adjust thresholds based on subsequent testing.*
Threshold parameters	Most thresholds in algorithm are hard-coded (in .c or .h files)	Most threshold parameters in algorithm are hard-coded.	*Place all threshold parameters in external configuration file*
Geometric search configuration	Parameters hard-coded in code Functions only with a single sensor geometry	N/A (Performs only a rectilinear search)	*Software interoperates with VIIRS and MODIS geometric characteristics, determined automatically from input file* *Geometric parameters for VIIRS sensor settable via configuration file*

Note:
Desert test described in reference paper is:

Reject fires along desert boundaries if

$N_f > 0.1\ N_v$ $N_f >= 4$

$\rho_{.86} > 0.15$ $T'_{4B} < 345$

$\delta'_4 < 3$ $T_4 < T'_{4B} + 6\ \delta'_4$

where N_v is the number of valid background pixels and N_f is the background fires in the search box